EXAMINATION OF TROPICAL CYCLONE STRUCTURE AND INTENSIFICATION WITH THE EXTENDED FLIGHT LEVEL DATASET (FLIGHT+) FROM 1999 TO 2012

A THESIS SUBMITTED TO THE GRADUATE DIVISION OF THE UNIVERSITY OF HAWAIʻI AT MĀNOA IN PARTIAL FULFILLMENT OF THE REQUIREMENTS FOR THE DEGREE OF

MASTER OF SCIENCE

IN

ATMOSPHERIC SCIENCES

MAY 2016

By

Jonathan Martinez

Thesis Committee:

Michael M. Bell, Chairperson
Gary Barnes
Yuqing Wang

Keywords: tropical cyclones, structure, intensification, aircraft composites

ACKNOWLEDGMENTS

I would like to thank the crews of both the 53rd Weather Reconnaissance Squadron and NOAA Aircraft Operations Center whose hours of hard work and dedication to collecting high quality observations in tropical cyclones made this research possible. I am deeply grateful for my adviser Michael Bell who provided me the amazing opportunity to seek my research interests under his guidance. His willingness to help and insightful conversations constantly motivated and challenged me to think critically of my work. Furthermore, funding my travel to three conferences was vital in allowing me to receive feedback from the scientific community, which significantly improved the work presented. I would also like to thank my committee members, Gary Barnes and Yuqing Wang, for their helpful comments and constructive criticism which challenged me to further improve my research. Gary's insightful questions constantly challenged my understanding and opened my mind to challenging the work of others. Yuqing provided me with fundamental knowledge of TCs through his unique TC class and helped me develop a deeper understanding of TCs through his teaching. A special thanks goes to Jonathan Vigh of the National Center for Atmospheric Research (NCAR) who created the wonderful FLIGHT+ dataset that made this research possible. I began this project under his advisement in the summer of 2014 through the Significant Opportunities in Atmospheric Research and Science (SOARS) program and am truly grateful for the help he provided, especially in teaching me how to code. I'd also like to thank Robert Rogers of the Hurricane Research Division (HRD)/Atlantic Oceanographic Meteorological Laboratory for his insightful comments which helped steer the direction of my research. A huge thanks goes out to the SOARS program for providing me the opportunity to begin this research under Jonathan Vigh's advisement. Conversations with Rebecca Haacker, Bec Batchelor, and Laura Allen helped shape me into a better student, scientist, and person. Their dedication to helping me through the research process and applying to graduate schools brought me further than I would've ever gone on my own. I would also like to thank my family and friends whose constant belief in my abilities motivated me to keep succeeding. Time spent with them during breaks kept me sane and the happiness they brought me throughout this journey was invaluable. Finally, I would like to thank my best friend, my father, whose endless belief in my potential to succeed often exceeded my own. He talked me through many stressful situations and always supported my vision. All of my accomplishments were made possible by his guidance and he was my true source of motivation. Therefore, I dedicate this work to my father, whose pride in me will always be felt.

ABSTRACT

A comprehensive examination of tropical cyclone (TC) kinematic and thermodynamic structure in the Atlantic basin is created from the Extended Flight Level Dataset (FLIGHT+) for Tropical Cyclones (Version 1.0). In situ data collected at the 700 hPa flight level by NOAA WP-3D and USAF WC-130 aircraft from 1999 to 2012 were analyzed. 233 flights consisting of 1491 total radial legs were stratified by TC intensity and 12 hour intensity change. A matrix of composite structures was then calculated for hurricanes (Categories 1 and 2 on the Saffir-Simpson scale) and major hurricanes (Categories 3 and above) that were intensifying [intensity increase $\geq$ 10 kt $(12\ \text{h})^{-1}$], steady-state [intensity change between $\pm$ 5 kt $(12\ \text{h})^{-1}$], and weakening [intensity decrease ≤ -10 kt $(12\ \text{h})^{-1}$]. Additional considerations to the age of TCs and a previous or future 12 h intensity change are given as well.

Axisymmetric radial composites reveal that intensifying TCs had statistically significant structural differences from TCs that were steady-state or weakening, but that these differences also depend on the intensity of the TC. Intensifying TCs were characterized by steep tangential wind gradients inside the radius of maximum tangential wind (RMW) that contributed to a ring-like structure of vorticity and inertial stability. Furthermore, intensifying TCs possessed the lowest absolute angular momentum compared to steady-state and weakening TCs. The composites indicated more tangential wind structural differences inside the RMW for hurricanes compared to major hurricanes. Thermodynamic structures showed fewer differences than the kinematic structures in general, but intensifying TCs were found to have higher moisture content outside the RMW overall.

TABLE OF CONTENTS

Acknowledgments . . . . . **iii**

Abstract . . . . . **iv**

List of Tables . . . . . **vii**

List of Figures . . . . . **ix**

1 Introduction **1**

1.1 Background 1

1.2 Research Objectives 6

2 Methods **8**

2.1 Description and stratification of Best Track data 8

2.2 Description and processing of flight level data 9

2.3 Large scale characteristics 16

2.4 Creation of the composite-mean structures 17

2.5 Stratification of results by TC age 18

2.6 Statistical significance testing 19

3 Axisymmetric kinematic composite-mean structures **21**

3.1 Tangential wind velocity 21

3.2 Radial wind velocity 22

3.3 Vertical vorticity 23

3.4 Inertial stability 24

3.5 Absolute angular momentum 26

4 Thermodynamic composite-mean structures 28

4.1 Temperature 28

4.2 Dewpoint temperature 29

4.3 Dewpoint depression 29

4.4 Equivalent potential temperature 30

5 Discussion 32

5.1 Gradients of tangential wind 32

5.2 Vorticity ring structure and outer-core vorticity 36

5.3 Absolute angular momentum 40

5.4 Thermodynamic structural differences 42

5.5 Large scale characteristics 45

5.6 Statistics evaluated at the RMW 47

6 Summary and conclusions 50

Bibliography 53

LIST OF TABLES

2.2 As in 2.1, but using a previous 12 h intensity change bin. 16

2.3 As in 2.1, but using a future 12 h intensity change bin. 16

2.1 Summary of the number of flights that were matched to a BT fix for each intensity and centered 12 h intensity change bin. The thresholds for each bin according to intensity and intensity change are described in Section 2.2. . . . 16

2.4 Large scale variables obtained from the SHIPS database. 17

2.5 Summary of the number of flights that were matched to a BT fix for each intensity, centered 12 h intensity change, and age bin. The thresholds for each bin according to intensity, intensity change, and age are described in Section 2.2. 19

5.1 Composite-mean flight age and normalized flight age for each intensity and centered 12 h intensity change bin. Standard deviations are given in parentheses. See section 2.5 for a description on how the normalized flight age was computed. 38

5.2 Composite large scale statistics evaluated from the SHIPS database for each bin using a centered 12 h intensity change. The composite-mean value for each bin is given along with the standard deviation in parentheses. Statistically significant differences at the 5% level using a two-tailed WMW rank-sum test are denoted by colored asterisks following the composite-mean value. Colors denote which composite-mean was significantly different from the given composite-mean and color coding follows that used in the composite-mean structure figures (i.e., blue = WK, green = SS, red = IN. For example, a red asterisk next to the composite-mean value of WK SST denotes that it was significantly different from IN SST at the 5% level. 47

5.3 Composite kinematic statistics evaluated in each bin at the RMW using a centered 12 h intensity change. The composite-mean value at the RMW for each variable is given along with the standard deviation in parentheses. Statistically significant differences at the RMW can be observed in the Figures presented in chapter 3. 48

5.4 Composite thermodynamic statistics evaluated in each bin at the RMW using a centered 12 h intensity change. The composite-mean value at the RMW is given for each variable along with the standard deviation in parentheses. Statistically significant differences at the RMW can be observed in the Figures presented in chapter 4. 49

LIST OF FIGURES

1.1 Adapted from Shea and Gray (1973). Tangential wind velocity for deepening storms (red; our inset) superimposed on the tangential wind velocity for filling storms (black), plotted as a function of radius with respect to the RMW. Solid curves denote the 900–700 mb layer and dashed curves denote the 700–500 mb layer. 7

2.1 N43RF flight 20040914I1 through Hurricane Ivan as it entered the Gulf of Mexico (a). The black lines denote the path of the aircraft, beginning and ending at the MacDill Air Force base in Tampa Bay, FL. The wind centers determined by HRD for the duration of the flight are shown in red. The "good" radial legs that were flown are shown as a function of the distance to the storm center (b) which is given by the hurricane symbol. 14

2.2 Storm-relative axisymmetric tangential wind velocity plotted as a function of radial distance for each of the good radial legs (denoted by different colors) and overlaid by the azimuthal mean (black) for flight 20040914I1 through Hurricane Ivan (a). (b) The azimuthal mean (gray) overlaid by the smoothed azimuthal mean (red). (c) The smoothed azimuthal mean plotted as a function of r^*. 14

2.3 Box-and-whisker plots for the RMW size (km) in each bin. The labels on the abscissa represent the intensity, denoted by the first letter ("H" for Hurricane and "MH" for Major Hurricane) followed by the intensity change bin (WK = Weakening, SS = Steady-State, IN = Intensifying). The red line denotes the median RMW size while the upper and lower edges of the box represent the upper ($q_{0.75}$) and lower ($q_{0.25}$) quartiles, respectively. Whiskers extend to $q_{0.75}$ + IQR and $q_{0.25}$ - IQR, where IQR represents the inter-quartile range ($q_{0.75}$ - $q_{0.25}$). Outliers are defined outside of the range covered by the whiskers and denoted by red crosses. 15

2.4 Storm-relative axisymmetric tangential wind velocity for each azimuthal mean (gray), overlaid by the composite-mean (red) for WK major hurricanes (a) and IN major hurricanes (b). 18

3.1 Storm-relative axisymmetric tangential wind velocity composite-means for hurricanes (a) and major hurricanes (b). Radial locations where all composite-means were significantly different at the 5% level are shaded in gray and two significantly different composite-means are denoted in bold. 22

3.2 As in Figure 3.1, but for storm-relative axisymmetric radial wind. 23

3.3 As in Figure 3.1, but for axisymmetric vertical vorticity. 24

3.4 As in Figure 3.1, but for axisymmetric inertial stability. 25

3.5 As in Figure 3.1, but for non-dimensional absolute angular momentum. . . . 27

3.6 As in Figure 3.1, but for dimensional absolute angular momentum. 27

4.1 As in Figure 3.1, but for temperature. 28

4.2 As in Figure 3.1, but for dewpoint temperature. 29

4.3 As in Figure 3.1, but for dewpoint depression. 30

4.4 As in Figure 3.1, but for equivalent potential temperature. 31

5.1 Storm-relative axisymmetric tangential wind velocity composite-means for early stage hurricanes (a) and major hurricanes (b), and late stage hurricanes (c) and major hurricanes (d). Radial locations where all composite-means were significantly different at the 5% level are shaded in gray and two significantly different composite-means are denoted in bold. 34

5.2 Storm-relative axisymmetric tangential wind velocity composite-means for hurricanes and major hurricanes using a previous 12 h intensity change (a and b, respectively) and hurricanes and major hurricanes using a future 12 h intensity change (c and d, respectively). Radial locations where all composite-means were significantly different at the 5% level are shaded in gray and two significantly different composite-means are denoted in bold. 35

5.3 As in Figure 5.1, but for axisymmetric vertical vorticity. 39

5.4 As in Figure 5.2, but for axisymmetric vertical vorticity. 40

5.5 As in Figure 5.1, but for dewpoint depression. 44

5.6 As in Figure 5.2, but for dewpoint depression. 45

CHAPTER 1
INTRODUCTION

1.1 Background

The structure of a tropical cyclone (TC) is influenced by both internal processes (e.g., convective bursts, eyewall replacement cycles, vortex Rossby waves, upper level outflow) and external processes (e.g., vertical wind shear, ocean surface temperatures and heat content, synoptic scale forcing). These physical processes are actively linked to the intensification of the TC and often manifest themselves as structural changes at various stages in the TC's life cycle. Therefore, understanding feedback mechanisms between TC structure and intensification remains crucial to improving our intensity forecasts for TCs.

Motivated to improve TC intensity forecasts, Kaplan and DeMaria (2003) developed the rapid intensification index (RII) for TCs in the north Atlantic basin by investigating the large scale characteristics associated with TCs that were rapidly intensifying during the period of 1989–2000. Rapid intensification (RI) was defined as the approximately 95th percentile of 24 hour intensity changes which corresponded to an intensity increase of 15.4 m s^{-1} (30 kt) over a 24 h period for TCs in the North Atlantic basin. They showed that using large scale characteristics as predictors, such as sea surface temperatures (SSTs), relative humidity averaged over a layer, and deep layer vertical wind shear (VWS) of the horizontal wind, a statistical technique for forecasting the probability of RI could be derived. Variables that were chosen as predictors for the RII had statistically significant differences between rapidly intensifying and non-rapidly intensifying TCs at the 5% level. Their method showed improvements over a purely climatological RI perspective and was used in real time during the 2001 Atlantic hurricane season to demonstrate it's viability. Kaplan et al. (2010) elaborated on the findings reported by Kaplan and DeMaria (2003) by implementing a linear discriminant analysis as a more statistically robust method to determine the probability of RI. Large scale characteristics in the Eastern North Pacific and North Atlantic basins were used as predictors for the onset of RI. Variables chosen as predictors were required to have statistically significant differences between RI and non-RI TCs at the 1% level. Furthermore, the RII was developed for three thresholds: 25, 30, and 35 kt intensity increases over a 24 hour period. Their method showed improvements in forecasting the onset of RI compared to Kaplan and DeMaria (2003) and its viability was measured with the Pierce skill score (PSS).

The PSS measures the difference between the probability of detection and the probability of false detection where a score of 1 represents a perfect forecast and a score of 0 represents a forecast that has no skill. The PSS for the RII ranged from approximately 0.1–0.4 in the Atlantic basin and approximately 0.45–0.65 in the Eastern North Pacific basin for the 2006 and 2007 seasons [cf. Figure 17 in Kaplan et al. (2010)]. Remaining uncertainties in forecasting RI were attributed to the lack of vortex and convective scale features included in the RII.

The foregoing discussion suggests the necessity to characterize the core structure of TCs to further understand the differences between TCs that intensify and those that do not. Observational research investigating the inner-core structure of TCs dates back to Shea and Gray (1973) who developed in situ (flight level) composite-mean structures of the inner-core region of TCs sampled during the National Hurricane Project between 1957–1969. They were one of the first to describe the inner-core structure of TCs: tangential winds decrease with height, the highest temperatures are found inside the RMW and often in the eye, and the strongest inflow occurs at lower levels in the boundary layer. A unique finding reported by Shea and Gray was the difference in the inner-core structure between deepening and filling storms. They noted that filling storms had larger vertical shearing flow resulting in less cumulus convection, which in turn inhibited the higher momentum from lower levels to be transported vertically. Figure 1.1 shows the tangential wind structures for deepening and filling storms, adapted from Shea and Gray (1973). Deepening storms exhibit a much steeper increase of tangential winds inside the RMW and a steeper decrease of tangential winds outside the RMW compared to filling storms.

Kossin and Eastin (2001) examined the kinematic and thermodynamic evolution of hurricanes Diana (1984) and Olivia (1994) using flight level data. Two distinct regimes were classified at different stages in the life cycles of both Diana and Olivia. The intensification phase was characteristic of "regime 1" which was thermodynamically denoted by a large dewpoint depression in the TC's eye and relatively elevated equivalent potential temperature (θ_e) in the eyewall. Kinematically, it was denoted by elevated angular velocity and relative vorticity in the eyewall. The transition to "regime 2" was defined as the phase proceeding the intensification phase of regime 1 (typically after maximum intensity was achieved) and was indicative of increased dewpoints in the eye which corresponded to a monotonic profile of θ_e. The transition to regime 2 was also associated with a relaxation of flow across the eye and eyewall which led to solid body rotation, increased tangential flow in the eye, and a monotonic structure of angular velocity and vorticity. Their results were said to be representative

of a larger sample of TCs and therefore, they concluded that these structural differences could potentially distinguish an intensifying TC from one that is no longer intensifying.

Kossin and Eastin (2001) attributed horizontal mixing across the eye and eyewall associated with the formation and breakdown of a vorticity ring (Schubert et al. 1999) as the possible mechanism for the observed transition from regime 1 to regime 2. Physical processes associated with the formation and destruction of an annular potential vorticity (PV) ring have been documented to impact the kinematic structure of TCs (Schubert et al. 1999). An annular PV ring structure for TCs satisfies the requirements for barotropic instability. That is, the radial gradient of PV is negative on the outer-edge of the PV ring and positive on the inner-edge. Vortex Rossby wave theory states that counter-propagating PV edge waves will form on the edges of the annulus. The PV wave that forms on the outer-edge will propagate clockwise relative to the local flow and the PV wave that forms on the inner-edge will propagate counterclockwise. The two waves can become phase-locked and this interaction may lead to amplification of both waves, resulting in exponential instability. Consequentially, the PV ring will breakdown and the radial structure of PV can be significantly altered by this process. Specifically, the PV is rearranged in a manner where the higher PV found in the ring is mixed inward into the eye while the weaker PV found near the eye is mixed outward, ultimately leading to a monotonic profile of PV. The rearrangement of PV also brought about a change in the radial structure of tangential winds. Steep tangential wind gradients were observed prior to the breakdown of the PV ring. Tangential winds increased in the eye and experienced an overall reduction in magnitude after the breakdown of the PV ring. Lee and Bell (2007) also found steep tangential wind gradients accompanied by a vorticity ring structure for Hurricane Charley (2004) during RI which transitioned to a flatter tangential wind profile and monopole vorticity structure after maximum intensity was achieved.

Shapiro and Willoughby (1982) used a balanced model to demonstrate that point sources of heating and momentum were most efficient at spinning up tangential winds if they were located at or slightly inward of the RMW. Specifically, isobaric height falls were most rapid inside the RMW for a point source of heating located radially inward of the RMW. The spin-up of tangential winds was greatest inside the RMW due to the sharp gradient of isobaric height falls in that region, leading to a contraction of the RMW. Furthermore, Shapiro and Willoughby (1982) demonstrated that the spin-up of tangential winds was more efficient with increasing storm intensity. Willoughby et al. (1982) stated that given an axisymmetric framework, point sources of heating could be viewed as rings of heating and they coined the previously described process as the "convective ring" paradigm. Observational evidence of

convective rings were presented by Willoughby et al. (1982) and Willoughby (1990) through the use of aircraft in situ measurements. Convective rings were observed as symmetric rings of vigorous convection that persisted throughout the intensification process described above. Willoughby (1990) concluded that convective rings were the primary mechanism driving tangential wind differences between intensifying and non-intensifying (or weakening) TCs. The presence or lack of a convective ring led to steep tangential wind gradients inside and outside the RMW for intensifying hurricanes and flatter tangential wind profiles for non-intensifying hurricanes, respectively.

Pendergrass and Willoughby (2009) assessed the significance of the tilt and radial location of a diabatic heating source to TC intensification rates using a balanced axisymmetric TC. They elaborated on the results presented by Shapiro and Willoughby (1982) through the use of a tilted heating source. The efficiency of the diabatic heating source contributing to intensification was found to be most sensitive to changes in TC intensity, consistent with Shapiro and Willoughby (1982), and size (measured by the RMW). Diabatic heating efficiency increased with increasing TC intensity and decreasing RMW size. Holding the size of the TC constant, higher intensities correspond to a reduction in the Rossby length and thus higher diabatic heating efficiencies. Holding the intensity constant, decreasing the size of the RMW increases local vorticity and inertial stability which corresponds to a reduction in the Rossby length and higher diabatic heating efficiencies. Since the intensity of a TC increases and the RMW contracts during intensification, a positive feedback mechanism was deduced if diabatic heating was held constant and the vortex shape remained the same. Increasing the tilt of the diabatic heating source resulted in less efficient spin-up of tangential winds due to the induced flow becoming more parallel to constant absolute angular momentum surfaces. However, the tilt of the diabatic heating source was found to have a weaker effect on TC intensification rates compared to TC intensity and size of the RMW, highlighting their relevance.

Results from Vigh and Schubert (2009) further elaborated on the importance of the radial location of a diabatic heating source, specifically in relation to the region of high inertial stability proposed by Schubert and Hack (1982), through use of a balanced vortex model derived from the Sawyer-Eliassen equations. They found that diabatic heating occurring within the high inertial stability region inside the RMW was most efficient for spinning up tangential winds. Furthermore, diabatic heating found in the high inertial stability region increased subsidence inside the radius of diabatic heating, giving rise to rapid warm core development. Subsequently, the formation of an eye removed diabatic heating from the high

inertial stability region and reduced the efficiency of intensification. However, intensification could proceed if the Rossby length was said to be sufficiently small. Vigh and Schubert (2009) also found that intensification rates increased for higher intensity storms with smaller spatial scales due to a reduction of the Rossby length contributing to higher diabatic heating efficiencies in regions of high inertial stability.

Structural differences between the inner-core region of TCs that are intensifying and remaining steady-state have also been examined through the use of Doppler radar derived composites for an axisymmetric framework (Rogers et al. 2013). The use of Doppler radar is advantageous in that it allows examination of the vertical structure of the TC provided that there are sufficient scatterers. Steady-state (SS) TCs were found to have relatively higher outer-core tangential wind velocities and vorticity which was said to be indicative of higher inertial stability in that region. The outer-core was defined in the region $r^* =$ 2–3, where r^* represented the radial coordinate normalized by the RMW at 2 km altitude (i.e., $r^* = r/RMW_{2km}$). Intensifying (IN) TCs exhibited a ring-like structure of vorticity (a vorticity maximum radially inward of the RMW) as shown for regime 1 TCs in Kossin and Eastin (2001). Furthermore, Rogers et al. (2013) demonstrated that convective bursts (CBs) were preferentially located inside the RMW for IN storms where the axisymmetric vorticity was higher, compared to outside the RMW for SS storms where the axisymmetric vorticity was lower. CBs were defined as the top 1% of the vertical velocity distribution at 8 km, corresponding to an updraft threshold of 5.5 m s^{-1} for both the IN and SS composites examined in their study. The radial location of CBs with respect to the RMW was highlighted as a key finding in their study and supports the results demonstrated in previous literature (Pendergrass and Willoughby 2009; Shapiro and Willoughby 1982; Vigh and Schubert 2009). That is, diabatic heating located in the region of high inertial stability (deduced from high vorticity) is more effective for TC spin-up.

Mallen et al. (2005) compared the observational axisymmetric radial structure of TCs to idealized profiles through the use of flight level composites from a large sample of TCs between 1977–2001. They demonstrated that realistic TCs possess a slow tangential wind decay outside the RMW, given by tangential wind decay exponents (α) of 0.31, 0.35, and 0.48 for pre-hurricanes, hurricanes, and major hurricanes, respectively. Tangential wind decay exponents were computed for a modified Rankine vortex and can be represented outside the RMW by $V = V_m(r_m/r)^\alpha$ where V represents the tangential wind, V_m represents the maximum tangential wind, r_m represents the RMW, and r represents the radius. The slow tangential wind decay outside the RMW corresponded to non-zero skirt of cyclonic vorticity

in that region. Mallen et al. (2005) argued that this intrinsic characteristic of TCs allowed them to survive weak to moderate vertical wind shear in contrast to the unrealistic idealized radial structures of modeled TCs. Interestingly enough, Gray and Shea (1973) found a similar decay exponent (0.47) for all of their combined radial legs between the 900–500mb layer.

A preponderance of observational and numerical case studies exist documenting the structural evolution of TCs in various environmental conditions and through various perspectives. These studies provide thorough examinations of the feedback processes occurring between the TC's structure and intensification. As stated by Shea and Gray (1973) and also observed in the data to be presented in this study, high variability exists on a case to case basis. The composite approach serves to identify robust structural characteristics amongst TCs stratified by certain parameters. Previous composite studies have placed an emphasis on distinguishing the structure of an intensifying TC from one that is remaining steady-state (Kossin and Eastin 2001; Rogers et al. 2013) or weakening (Shea and Gray 1973; Willoughby 1990). Distinct features were found when TCs were stratified by intensity change, but they did not stratify their results by the TC's intensity. As demonstrated by Shapiro and Willoughby (1982), Pendergrass and Willoughby (2009), and Vigh and Schubert (2009), the intensity of a TC plays an important role on determining the efficiency of intensification. Mallen et al. (2005) investigated the outer-core tangential wind structure of TCs stratified by intensity, however in their case, they did not stratify by the intensity change of their sampled TCs.

1.2 Research Objectives

I hypothesize that the consideration of both intensity and intensity change would reveal kinematic and thermodynamic structural differences between composites of TCs that have previously not been observed due to the consideration of only one or the other. Furthermore, I hypothesize that considering the age of the TC may also give rise to distinct kinematic and thermodynamic structural differences between TCs that are in early or late stages of their life cycle. My primary objective is to test the validity of these hypotheses through the creation of axisymmetric flight level composite structures. Additionally, I will determine if the composite-mean structural differences are statistically significant. To address these hypotheses, I will use flight level kinematic and thermodynamic measurements gathered by the National Oceanic and Atmospheric Administration (NOAA) WP-3D and the United States Air Force (USAF) WC-130 aircraft during flight missions through TCs. Flight level

data collected from 1999 to 2012 were obtained from the Extended Flight Level (FLIGHT+) Dataset for Tropical Cyclones (Version 1.0) created by Vigh et al. (2016). This extensive flight level database allows for stratification of results by intensity, intensity change, and age while maintaining sufficiently large sample sizes. The organization of this thesis is as follows: chapter 2 thoroughly discusses the data and methodology used to create the flight level composites. The kinematic structures of the composite-means are discussed in chapter 3 and the thermodynamic structures are discussed in chapter 4. A discussion of the physical processes pertaining to the results will be provided in chapter 5 and a summary of the work will be presented in chapter 6.

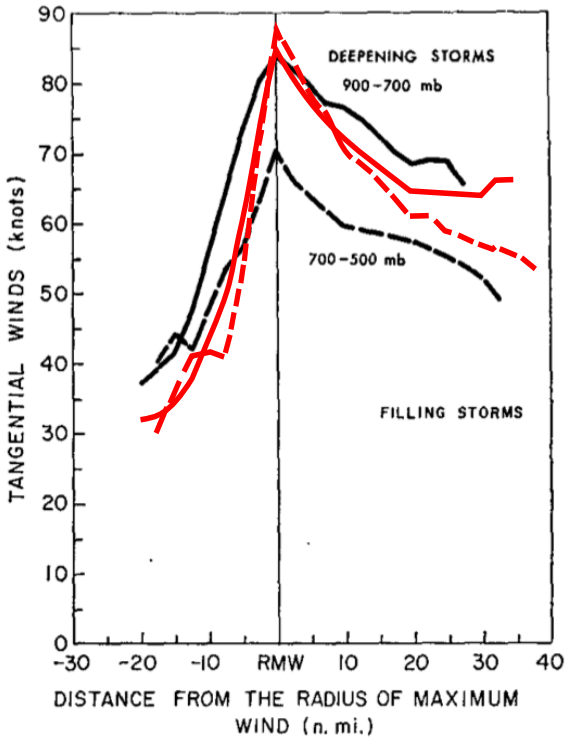

Figure 1.1: Adapted from Shea and Gray (1973). Tangential wind velocity for deepening storms (red; our inset) superimposed on the tangential wind velocity for filling storms (black), plotted as a function of radius with respect to the RMW. Solid curves denote the 900–700 mb layer and dashed curves denote the 700–500 mb layer.

CHAPTER 2
METHODS

2.1 Description and stratification of Best Track data

TC intensity and 12 h intensity change were determined using the National Hurricane Center's Best Track (BT) database for TCs in the North Atlantic basin from 1999 to 2012. BT data are organized as 6-hourly "fixes" during the life cycle of a TC. These fixes are typically created at standard synoptic times (i.e., 0000, 0600, 1200, and 1800 UTC), however, exceptions are sometimes made in the event of land falling TCs. For the purpose of this study, the structures of land falling TCs were not of interest and were thus excluded. The following section further discusses the method involved in determining the TC's distance to land and how it was utilized in removing landfalling TCs from the analysis. Cases of extra-tropical transition were also removed from the BT data. BT fixes that did not have a synoptic reference time were removed from the analysis. The BT intensity (BT $v_{\max}$) is defined as the maximum 1-min sustained wind speed at 10 m given in knots (1 kt = 0.51 m s^{-1}). This variable was used to calculate TC intensity and 12 h intensity change centered around the time of a given BT fix. For example, the intensity change of a TC with a BT fix reported at 1200 UTC would take the difference of BT $v_{\max}$ at 1800 and 0600 UTC. A centered time difference for intensity change best represented the physical processes impacting the structure of the TC at the time it was weakening, remaining steady-state, or intensifying. Results obtained when using a previous or future 12 h intensity change were also addressed using the same methodology and yielded similar results. Chapter 5 will include results derived using a previous and future 12 h intensity change to augment the main results obtained using a centered 12 h intensity change.

Organization of BT fixes by intensity and 12 h intensity change proceeded after applying the aforementioned data removal. Two intensity and three intensity change bins were created according to the BT $v_{\max}$ and centered 12 h intensity change, giving a total of six possible bin permutations for the BT fixes. Intensity bins were defined for hurricanes (64 kt $\leq$ BT $v_{\max} \leq$ 95 kt) and major hurricanes (BT $v_{\max} >$ 95 kt) according to the Saffir-Simpson scale used for TCs in the Atlantic and Eastern North Pacific. The Saffir-Simpson scale classifies the intensity of TCs by the maximum sustained 1-min wind speed measured 10 m above the surface, identical to the definition of BT $v_{\max}$. As defined, the hurricane bin contains

Category 1 and 2 hurricanes and the major hurricane bin contains Category 3 and above major hurricanes. The centered 12 h intensity change bins were defined as intensifying [IN, intensity increase $\geq$ 10 kt (12 h)$^{-1}$], steady-state [SS, intensity change between $\pm$ 5 kt (12 h)$^{-1}$ inclusive], and weakening [WK, intensity decrease $\leq$ -10 kt (12 h)$^{-1}$]. The IN and SS bin thresholds were similar to those in Rogers et al. (2013) who instead used an intensity change calculated over 12 h that was then extrapolated to a 24 h intensity change.

2.2 Description and processing of flight level data

The structure of TCs were examined using in situ data from the FLIGHT+ dataset (Vigh et al. 2016), a comprehensive database containing in situ (flight level) data recorded by the NOAA WP-3D and USAF WC-130 aircraft during flight missions through TCs. In the context of this study, TC structure will be referred to as the changes of a given variable in the radial direction ($\partial/\partial r$) from the TC center. The average date and time of each flight in the database were rounded to the nearest synoptic time and flights were subsequently matched to BT fixes binned by intensity and intensity change. Aircraft missions into TCs are typically flown at either the 850 or 700 hPa pressure level. The 700 hPa pressure level was chosen for this study due to the small number of flights at the 850 hPa level into TCs of hurricane or major hurricane intensity.

Data provided in the FLIGHT+ dataset were either indexed by time or interpolated to radius in 100 m bins. The location of the wind centers for the duration of each flight were determined using the objective center tracking algorithm described by Willoughby and Chelmow (1982). The storm motion vector can be derived by differentiating the track of the wind center for each flight. Subtracting the storm motion vector from the earth-relative wind field provided storm-relative winds, which were used in this study. As discussed by Willoughby and Chelmow (1982), the center tracking algorithm provided wind center locations within 3 km accuracy and storm motion vectors averaged over four to six hours with 4° directional accuracy and 0.5 m s^{-1} speed accuracy. Errors in the location of the wind center are ultimately introduced as errors in the storm-relative wind velocities. Typically, these errors are concentrated near the eye of the TC and are more prominent in the storm-relative radial wind velocities, but storm-relative tangential wind velocities are affected as well. Storm-relative winds provided in version 1.0 of the FLIGHT+ dataset may contain errors due to an incorrect calculation of the zonal and meridional components of the storm motion vector. Errors up to twice the translation speed may have been introduced into the

storm-relative wind velocity calculations (Jonathan Vigh; personal communication). Such errors may be random in nature, however a systematic component also exists given that TCs moving in the same direction will possess similar errors in their storm-relative winds. The kinematic results presented in this study make use of the storm-relative tangential winds and therefore these errors may be present in the analysis. The kinematic results will be recomputed in the near future with an updated version of the FLIGHT+ database that correctly computes the zonal and meridional components of the storm motion vectors. Results presented in this analysis will be compared to those regenerated with the updated dataset to determine if the errors significantly contributed to the results. It is believed that these errors have not significantly contributed to the results presented given that the averaging and compositing procedures discussed later in this section have likely averaged out significant errors introduced into independent cases. Kinematic results were reproduced using earth-relative winds which yielded nearly identical results, which further supports this argument.

Corrections were applied to both temperature and dewpoint temperature for each radial leg prior to any thermodynamic computations. Errors in temperature and dewpoint measurements can be introduced from instrument wetting which can cause an underestimation of temperature and an overestimation of dewpoint temperatures (Zipser et al. 1981). In the case of temperature, instrument wetting can cause evaporative cooling to occur on the thermistor, leading to a reduced temperature measurement. As for dewpoint, wetting on the hygrometer causes the thermoelectric circuit to responsively increase the temperature to evaporate the water, leading to an overestimation of dewpoint temperatures. Zipser et al. (1981) developed a method to reduce the errors introduced by instrument wetting. Specifically, this method reduced errors that caused temperature values to be lower than dewpoint temperatures. This method involved adjusting the temperature and dewpoint to the average of the two and assuming saturation for all instances where the dewpoint temperature exceeded the temperature. The method was termed the Zipser-Meitin-LeMone (ZML) correction in literature and as discussed in detail by Eastin et al. (2002), is a method that was formulated to *reduce* the errors associated with instrument wetting, not to completely remove them. The ZML correction was applied to the temperature and dewpoint data for each radial leg in the dataset utilized for this study. A more accurate temperature correction could be applied to the NOAA WP-3D data through a method involving the radiometer derived temperatures, as done in an earlier study by Barnes et al. (1981). However, radiometer derived temperature data is not available for the USAF WC-130 and therefore this correction

was not applied to maintain consistency within the data analysis. Application of the ZML correction was found to reduce the average errors found during instrument wetting events by 30–50%, corresponding to an average temperature and equivalent potential temperature error of 0.6 and 2.7 °C, respectively (Eastin et al. 2002).

The azimuthal mean structure of each flight was calculated by averaging all of the radial legs in a given flight at each radial point. Figure 2.1 illustrates an example flight path from a flight taken into Hurricane Ivan (2004) by the NOAA WP-3D (N43RF) aircraft. N43RF flew multiple radial legs through the center of Ivan during this flight, although as shown in Figure 2.1b, only 8 radial legs were included in the analysis. Radial legs are defined as an inbound flight path towards the center or an outbound flight path away from the center of a TC. "Good" radial legs required the aircraft to pass through the center of the TC and those that did not meet this requirement were not included in the analysis. Additionally, radial legs were investigated individually to remove erroneous data. This was completed by observing profiles of tangential wind, temperature, and dewpoint temperature (after the ZML correction was applied) for each radial leg. Erroneous data were defined as radial legs that contained artificial features in tangential wind, temperature, or dewpoint that may have resulted from instrumentation errors. Common errors included near zero tangential winds for an entire radial leg, artificial (wave-like) fluctuations in dewpoint temperature, and temperature or dewpoint temperature values that were constant for the entire radial leg. These radial legs were hand-removed prior to the analysis. Continuing with the example flight through Hurricane Ivan, eight radial legs were included in the calculation of the azimuthal mean for this specific flight. A minimum of two good radial legs for a given flight were required for the calculation of the azimuthal mean and inclusion in the analysis.

Azimuthal means were then smoothed using a one dimensional 10 km Lanczos filter to remove small scale transient features. Further details regarding the specific methodology of Lanczos filtering can be found in Duchon (1979). The radial coordinate for each azimuthal mean was then normalized by the 700 hPa RMW of that azimuthal mean. Continuing with the example flight through Hurricane Ivan, Figure 2.2 illustrates the process listed above. Axisymmetric storm-relative tangential wind velocity was plotted as a function of radial distance from the center of Ivan for each of the steps in this process. Figure 2.2a shows the tangential wind speed profiles for the eight radial legs flown through Ivan, where each radial leg is denoted by a different color, and the azimuthal mean is overlaid in black. The azimuthal mean is also shown in Figure 2.2b (gray) overlaid by the smoothed azimuthal mean (red). This figure demonstrates the efficiency of the filter in removing small-scale features and

retaining the shape of the azimuthal mean profile. After the smoothed azimuthal means were created, normalizing the radial coordinate by the 700 hPa RMW was carried out and is shown for the same flight through Ivan in Figure 2.2c. The normalization of the radial coordinate was also observed to retain the overall shape of the azimuthal mean profile. Normalization of the radial coordinate has been widely utilized in previous literature (Shea and Gray 1973; Mallen et al. 2005; Rogers et al. 2013) for the creation of composites. This method establishes a common RMW reference point where the RMW occurs at a normalized radius of one for each azimuthal mean. As mentioned by Shea and Gray, this methodology places an emphasis on the inner-core region of TCs by separating the dynamically different regions inside and outside the RMW. However, this method also contains inherent drawbacks. Normalizing the radial coordinate by the RMW obscures any information relating to the size of the TC. Furthermore, if there is large variability in the size of the RMWs, then normalization of the radial coordinate will ultimately result in averaging across different radii when computing the composite-means. Figure 2.3 provides insight to the degree of variability in RMW sizes for the data analyzed using a centered 12 h intensity change. From this figure it is apparent that the RMW size is quite variable for the flights analyzed in this study. Therefore, it is important to consider both the benefits and drawbacks associated with the normalization method (listed above) when examining the results presented in this analysis. For simplicity, the smoothed, radially normalized azimuthal means will henceforth be referred to as "flights" and the normalized radius coordinate will be given as r^*.

The distance-to-land parameter provided by the Statistical Hurricane Intensity Prediction Scheme (SHIPS) database was used to determine the distance between the center of the TC and the nearest major land mass. This parameter was evaluated at the average time of the flight and at the previous/future 6 hours from this time, providing information about the TC's distance to land for the duration of the centered 12 h intensity change. When using a previous or future 12 h intensity change, this parameter was evaluated at the average time of the flight and at the previous or future 12 h from this time, respectively. A land threshold was then created to exclude TCs that were significantly interacting with land at any time during the 12 h intensity change window. The land threshold was created after determining the RMW for each flight, adding a 20 km buffer to the RMW, and then comparing this buffered RMW to the SHIPS distance-to-land parameter. If the buffered RMW distance for a given flight was greater than the SHIPS distance-to-land at any time during the centered 12 h intensity change, then the flight was not considered in the analysis. The RMW buffer was chosen to represent the TC eyewall region of each flight to a first order approximation.

Results were not sensitive to changes resulting from increasing the size of the buffer (i.e., removing additional flights from the analysis). The land thresold removes TCs that were land falling and TCs whose eyewalls were over land at any point during the 12 h intensity change period. Considering the aforementioned time, flight level, and distance-to-land information for each flight, a total of 233 flights comprised of 1491 radial legs through TCs from 1999 to 2012 were analyzed using a centered 12 h intensity change. Table 2.1 highlights the number of flights that were matched to binned BT fixes using the previously mentioned thresholds for intensity and a centered 12 h intensity change. Varying the intensity change calculation consequentially led to slightly different bin sizes compared to those given a centered 12 h intensity change. A total of 261 flights comprised of 1698 radial legs were analyzed when considering a previous 12 h intensity change, and 218 flights comprised of 1382 radial legs were analyzed when considering a future 12 h intensity change. Tables 2.2 and 2.3 give the number of flights in each bin when using a previous and future 12 h intensity change, respectively.

The Coriolis parameter was evaluated for each individual flight. This was accomplished through the use of the latitude of the RMW recorded for each radial leg. An average flight latitude was created by taking the average of the RMW latitude for all radial legs in a given flight. This flight average latitude was then used to calculate the Coriolis parameter for each flight, given as $f = 2\Omega \sin(\phi)$, where $\Omega = 7.292 \times 10^{-5}$ s^{-1} and ϕ = latitude (degrees). This Coriolis parameter was used in the calculation of inertial stability and absolute angular momentum described in chapter 3.

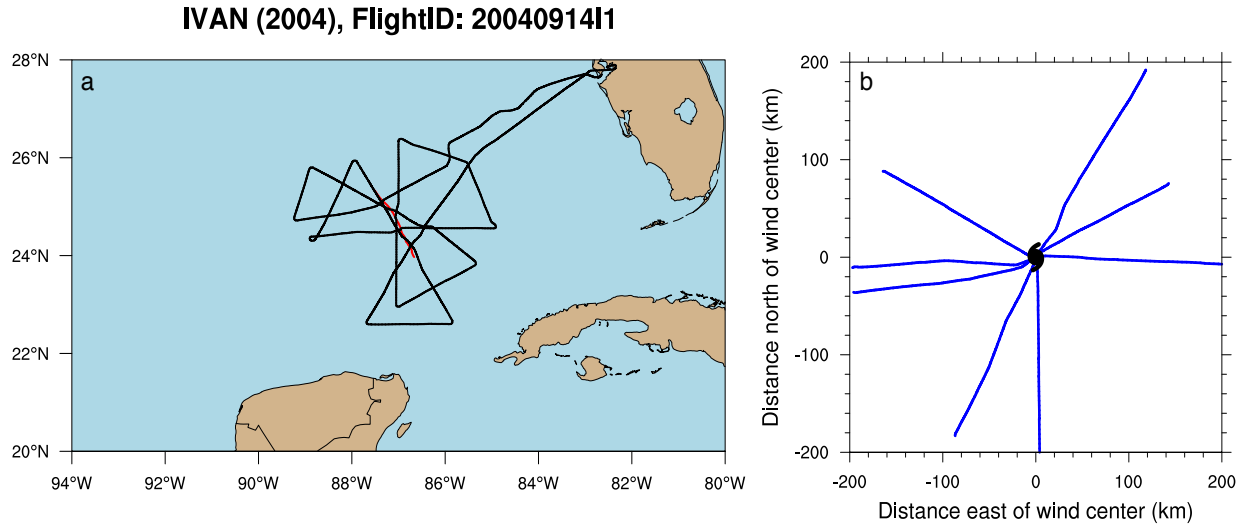

Figure 2.1: N43RF flight 20040914I1 through Hurricane Ivan as it entered the Gulf of Mexico (a). The black lines denote the path of the aircraft, beginning and ending at the MacDill Air Force base in Tampa Bay, FL. The wind centers determined by HRD for the duration of the flight are shown in red. The "good" radial legs that were flown are shown as a function of the distance to the storm center (b) which is given by the hurricane symbol.

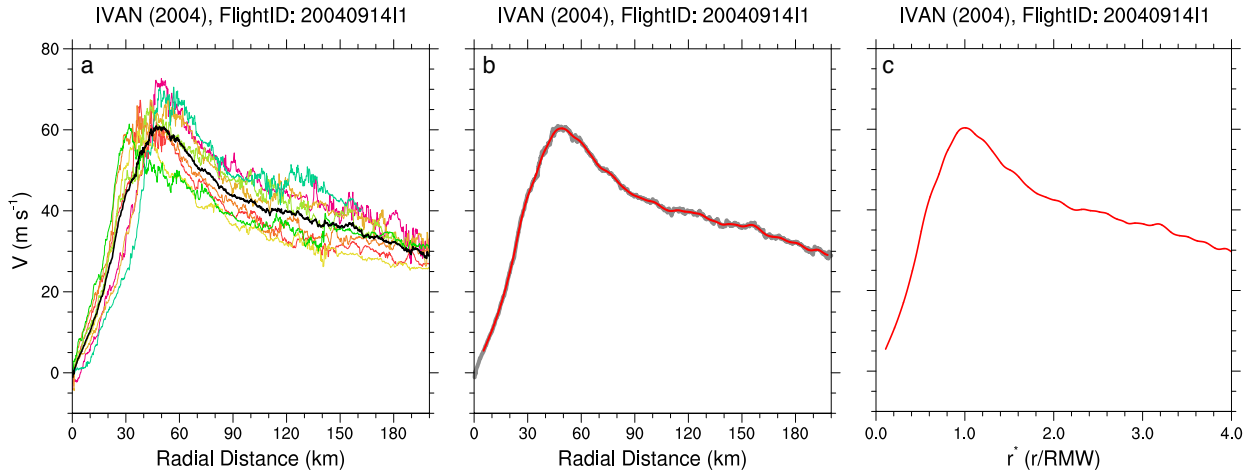

Figure 2.2: Storm-relative axisymmetric tangential wind velocity plotted as a function of radial distance for each of the good radial legs (denoted by different colors) and overlaid by the azimuthal mean (black) for flight 20040914I1 through Hurricane Ivan (a). (b) The azimuthal mean (gray) overlaid by the smoothed azimuthal mean (red). (c) The smoothed azimuthal mean plotted as a function of r^*.

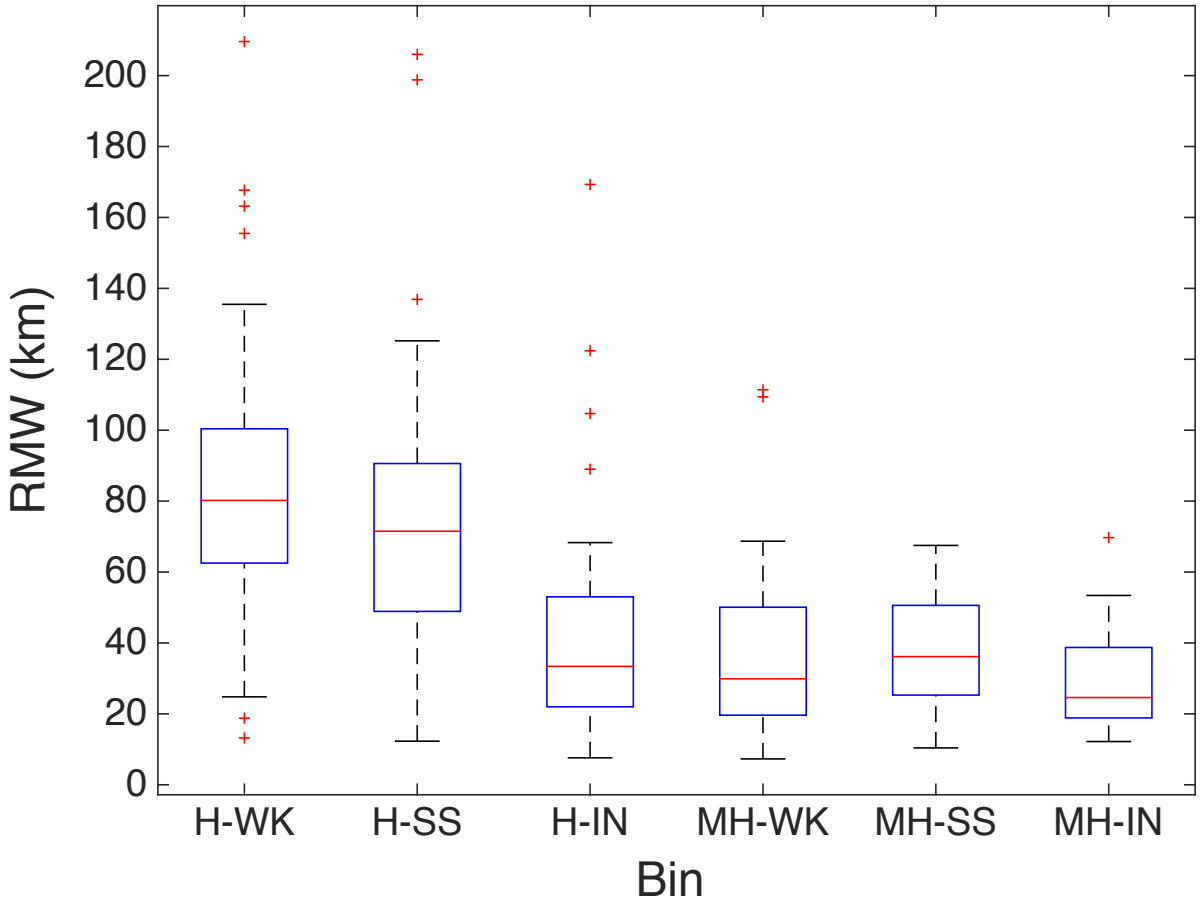

Figure 2.3: Box-and-whisker plots for the RMW size (km) in each bin. The labels on the abscissa represent the intensity, denoted by the first letter ("H" for Hurricane and "MH" for Major Hurricane) followed by the intensity change bin (WK = Weakening, SS = Steady-State, IN = Intensifying). The red line denotes the median RMW size while the upper and lower edges of the box represent the upper ($q_{0.75}$) and lower ($q_{0.25}$) quartiles, respectively. Whiskers extend to $q_{0.75}$ + IQR and $q_{0.25}$ - IQR, where IQR represents the inter-quartile range ($q_{0.75}$ - $q_{0.25}$). Outliers are defined outside of the range covered by the whiskers and denoted by red crosses.

Table 2.1: Summary of the number of flights that were matched to a BT fix for each intensity and centered 12 h intensity change bin. The thresholds for each bin according to intensity and intensity change are described in Section 2.2.

	Hurricane	Major Hurricane
WK	23	31
SS	48	46
IN	44	41

Table 2.2: As in 2.1, but using a previous 12 h intensity change bin.

	Hurricane	Major Hurricane
WK	21	33
SS	59	50
IN	47	51

Table 2.3: As in 2.1, but using a future 12 h intensity change bin.

	Hurricane	Major Hurricane
WK	18	31
SS	55	46
IN	38	30

2.3 Large scale characteristics

As discussed in chapter 1, the structure of a TC is influenced by internal and external processes. To assess the possible impacts of the large scale environment in which the TCs were embedded, additional large scale variables were examined from the SHIPS database. A summary of the variables selected and their descriptions are provided in Table 2.4. These variables were chosen to represent large scale characteristics that are likely to differ between hurricanes and major hurricanes that are WK, SS, or IN.

Table 2.4: Large scale variables obtained from the SHIPS database.

Variable	Description
RSST	Reynolds sea surface temperature (SST).
RHLO	850–700 hPa relative humidity from r = 200 to 800 km.
SHDC	850–250 hPa vertical shear magnitude from r = 0 to 500 km.
T200	200 hPa temperature from r = 200 to 800 km.

2.4 Creation of the composite-mean structures

With each of the six bins constructed and the flight level data processed using the previously mentioned methodology, the composite-mean structures were computed for each bin. Prior to the creation of the composite-means, the radially normalized, smoothed azimuthal mean profiles were linearly interpolated to a common radius space to allow the RMW to occur at a common normalized radius of one for each flight. The composite-means were constructed by simply averaging all of the flights in a given bin across all radii. Figure 2.4 provides insight to the process of creating the composite-means from the individual flights in each bin. It's important to note that the composite-mean structure of derived kinematic variables (vorticity, inertial stability, and absolute angular momentum) were created as composited quantities from the individual azimuthal mean structures. In other words, the composite-mean structures of these variables are not calculated using the radial derivative of the tangential wind composite-mean. For example, the composite-mean vorticity was calculated for each azimuthal mean and then followed the compositing methodology listed above. Hereafter, TCs will be referred to as either hurricanes or major hurricanes in their respective context to avoid confusion when mentioning results from different bins. Generalizations to the inclusive "TCs" will be made if results are common amongst both intensity bins.

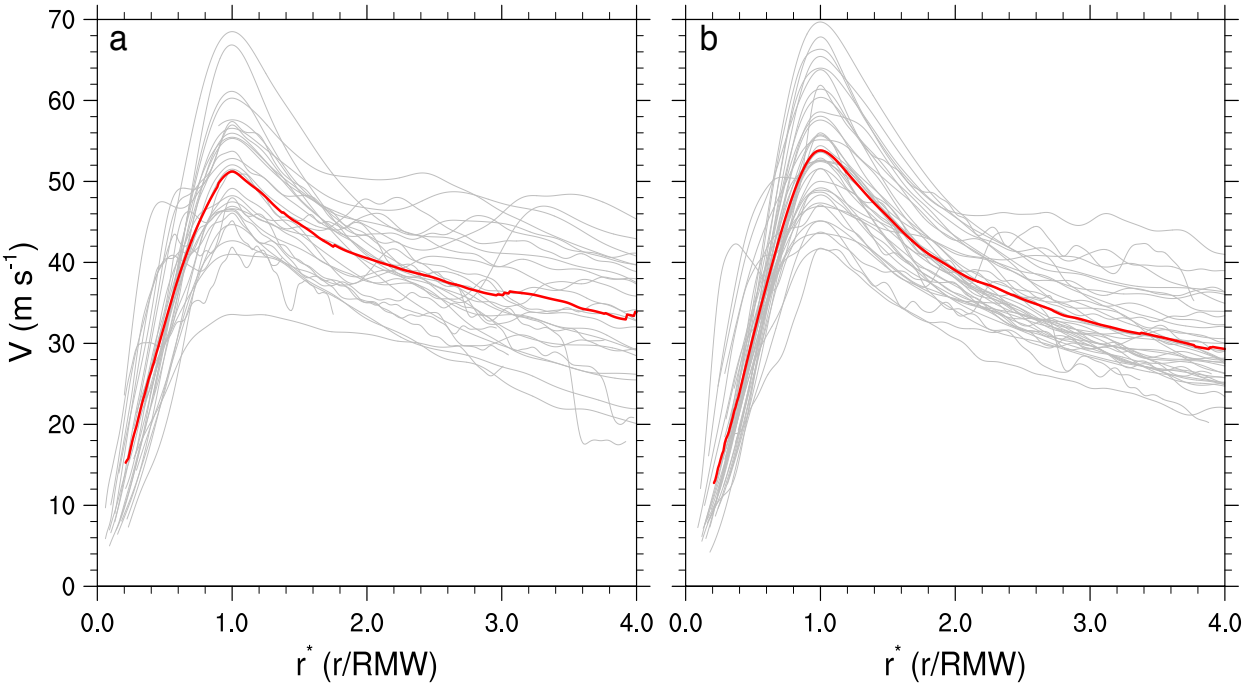

Figure 2.4: Storm-relative axisymmetric tangential wind velocity for each azimuthal mean (gray), overlaid by the composite-mean (red) for WK major hurricanes (a) and IN major hurricanes (b).

2.5 Stratification of results by TC age

Each of the flights that were previously binned by intensity and centered 12 h intensity change were further stratified according to the age of the TC at the time of the flight. TC age was first computed through use of the BT fix times. TC genesis was defined as the time of the first reported BT fix for a given TC. The maximum age of a TC was defined as the time of the last BT fix (excluding extra-tropical transition) reported for a TC. The life cycle of a TC was then computed by subtracting the genesis time from the maximum age time. The flight age of a TC (age of the TC at the average flight time discussed in section 2.1) was computed by subtracting the genesis time from the flight time. This flight age was then normalized by the lifetime of the TC. This method was invoked to provide insight to where the TC was in its life cycle in relation to the flight time. For example, if a TC had a lifetime of 10 days and a flight age of 5 days, a normalized flight age of 0.5 would demonstrate that the TC was half way through its life cycle at the time of the flight. Bin-average normalized flight ages were computed for each of the six bins by taking the average of all the normalized

Table 2.5: Summary of the number of flights that were matched to a BT fix for each intensity, centered 12 h intensity change, and age bin. The thresholds for each bin according to intensity, intensity change, and age are described in Section 2.2.

	Hurricane		Major Hurricane	
	Early	Late	Early	Late
WK	10	13	17	14
SS	19	29	23	23
IN	25	19	21	20

flight ages in a given bin. These bin-average normalized flight ages were then used to stratify the flights according to their normalized flight age. Early stage TCs were defined as a flight that had a normalized flight age less than the bin-average normalized flight age for the bin in which it was contained. Late stage TCs were defined similarly as flights that had a normalized flight age greater than the bin-average normalized flight age for the bin in which it was contained. The stratification of flights by TC intensity, centered 12 h intensity change, and age provided 12 possible bins for each flight. Table 2.5 highlights the number of flights (sample size) in each of these bins from this stratification. While this reduces the number of flights in each bin, some statistically significant and physically relevant results can still be obtained. It should be noted that the additional stratification by TC age was only carried out for the centered 12 h intensity change results.

2.6 Statistical significance testing

After the composite-means were created for each of the six bins, a two-tailed Wilcoxon-Mann-Whitney (WMW) rank-sum test was carried out to determine radial locations of statistically significant differences amongst the composite-mean structures at the 5% level. Given an intensity bin or intensity change bin, the WMW rank-sum test was carried out three times at each radial point to determine whether composite-means of WK, SS, or IN TCs were significantly different from each other. This placed an emphasis on the statistically significant differences across the intensity change spectrum. The null hypothesis for the test is that the two samples have been drawn from the same distribution. Rejection of the null hypothesis (i.e., acceptance of the alternative hypothesis) implies that the two samples were not drawn from the same distribution and are thus significantly different from each other. The WMW rank-sum test is a powerful nonparametric statistical significance test that is

resistant to outliers in the sampling distributions and nearly as robust as the Student's t test even when all assumptions for the t test are met. For a detailed explanation on the methodology involved in the WMW rank-sum test, the reader is directed to Chapter 5 of Wilks (2011).

CHAPTER 3
AXISYMMETRIC KINEMATIC COMPOSITE-MEAN STRUCTURES

3.1 Tangential wind velocity

The storm-relative axisymmetric tangential wind velocity composite-means for each bin are provided in Figure 3.1. The panels were constructed such that the composite-means could be plotted as a function of intensity change for each intensity bin. As previously mentioned, this method allowed for the comparisons of each composite-mean with an emphasis on the differences found across the intensity change spectrum. Radial locations where two or more composite-means had statistically significant differences at the 5% level using a two-tailed WMW rank-sum test are highlighted in bold on the composite-mean curves. Locations where all three composite-means were significantly different from each other are shaded in gray (labeled 3 significant differences below the figure). Radial regions within the TCs are specified here to simplify the discussion of the results. The eye is said to be found radially inward of $r^* = 0.6$, the inner-core lies between $r^* = 0.6$–2, and the outer-core lies outside of $r^* = 2$.

The hurricane composite-mean tangential wind profiles exhibited the greatest tangential wind differences in the eye, where IN hurricanes had the steepest increase of tangential winds followed by SS and then WK hurricanes. The magnitude of the statistically significant tangential wind differences in the eye of hurricanes was on the order of 2–6 m s^{-1}. Tangential wind differences in the inner and outer-core regions for hurricanes were minimal. Contrary to the tangential wind composite-mean structures for hurricanes, major hurricanes did not show many significant differences inside the RMW. They exhibited the most tangential wind differences in the outer-core region where WK major hurricanes possessed the shallowest decay of tangential wind velocity followed by SS and then IN major hurricanes. Statistically significant differences in outer-core tangential wind velocity were on the order of 2–4 m s^{-1}.

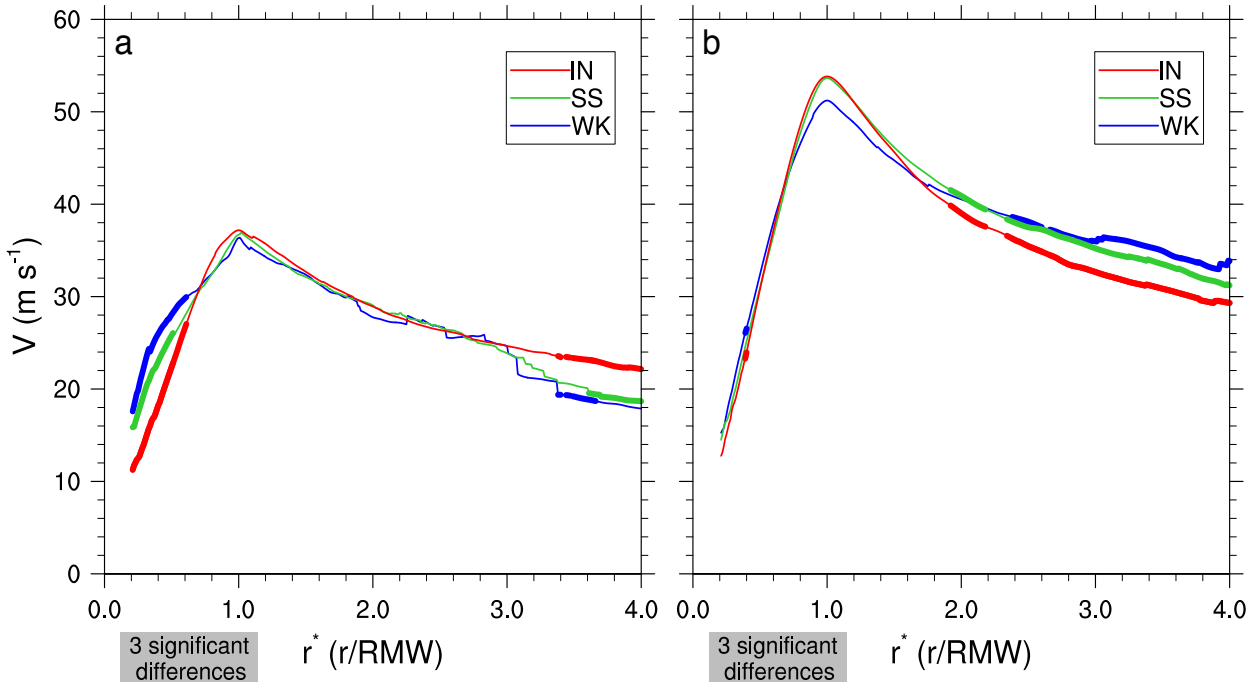

Figure 3.1: Storm-relative axisymmetric tangential wind velocity composite-means for hurricanes (a) and major hurricanes (b). Radial locations where all composite-means were significantly different at the 5% level are shaded in gray and two significantly different composite-means are denoted in bold.

3.2 Radial wind velocity

Figure 3.2 illustrates the composite-mean structures of storm-relative radial wind for each bin, similar to the layout in Figure 3.1. Since data collected at the 700 hPa flight level was used in this study, the magnitude of radial wind is weak, remaining between $\pm$ 2 m s^{-1} at all radii. Furthermore, there were almost no statistically significant differences found in the composite-mean structures of radial wind for either hurricanes or major hurricanes, suggesting it is not a distinguishing structure for intensity change at the 700 hPa flight level. All TCs exhibited an increase of weak radial outflow directly inside the RMW, characteristic of the outflow structure found above the inflow layer. Hurricanes have predominantly weak radial inflow in the outer-core region compared to major hurricanes which have predominantly weak radial outflow in that region.

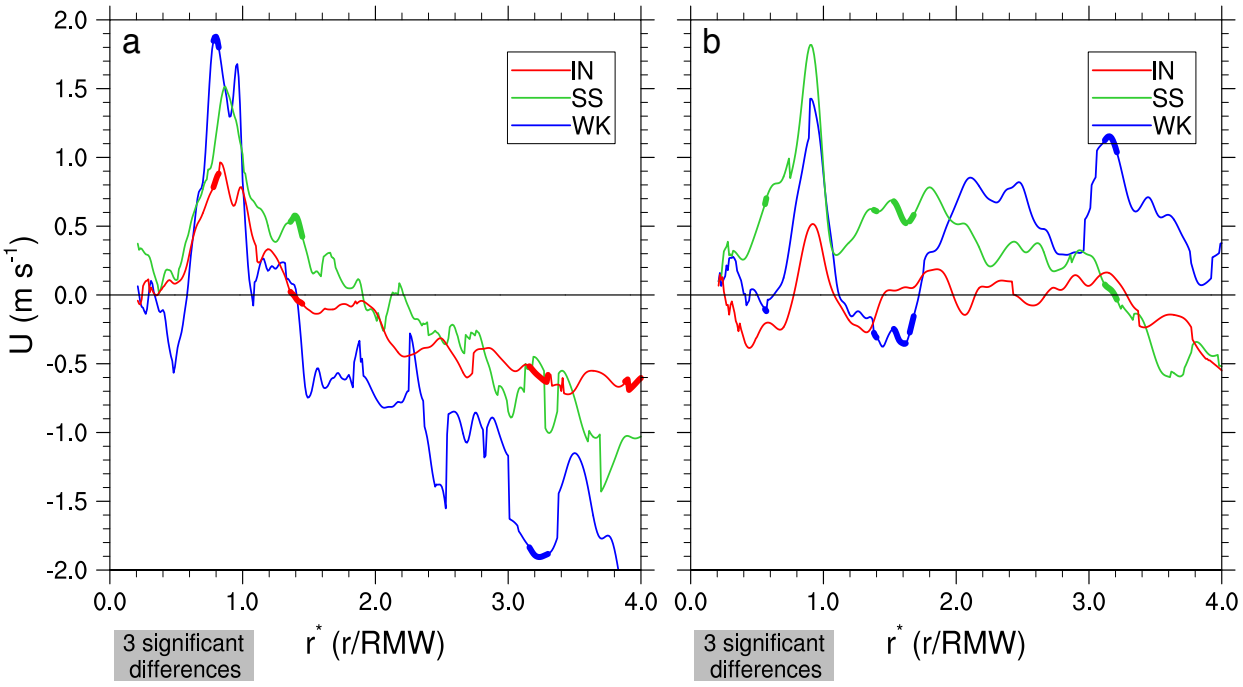

Figure 3.2: As in Figure 3.1, but for storm-relative axisymmetric radial wind.

3.3 Vertical vorticity

Axisymmetric vertical vorticity was computed from the smoothed azimuthal mean storm-relative axisymmetric tangential wind profiles and is given by

$$\zeta = \frac{\bar{V}}{r} + \frac{\partial \bar{V}}{\partial r} \tag{3.1}$$

where $\bar{V}$ represents the smoothed azimuthal mean storm-relative axisymmetric tangential wind velocity and r is the radial distance. Figure 3.3 shows the axisymmetric vertical vorticity composite-means for each bin. In general, IN TCs (hurricanes and major hurricanes) possessed a ring-like structure of vorticity with vorticity maximized radially inward of the RMW. IN hurricane vorticity was significantly higher than both SS and WK hurricane vorticity in the eye and inner-core region. The magnitude of the statistically significant differences in the eye ranged from 4×10^{-4} s^{-1} to twice that found in the eye when comparing IN hurricanes to SS or WK hurricanes. WK major hurricanes also possessed a vorticity ring structure in the eye while SS major hurricanes possessed a flatter vorticity profile, indicative of a more stable regime. Statistically significant differences in eye vorticity for IN major

hurricanes compared to SS major hurricanes ranged between approximately 10–20$\times 10^{-4}$ s^{-1}. Overall, major hurricanes possessed nearly twice the vorticity in the eye compared to hurricanes for each respective intensity change bin.

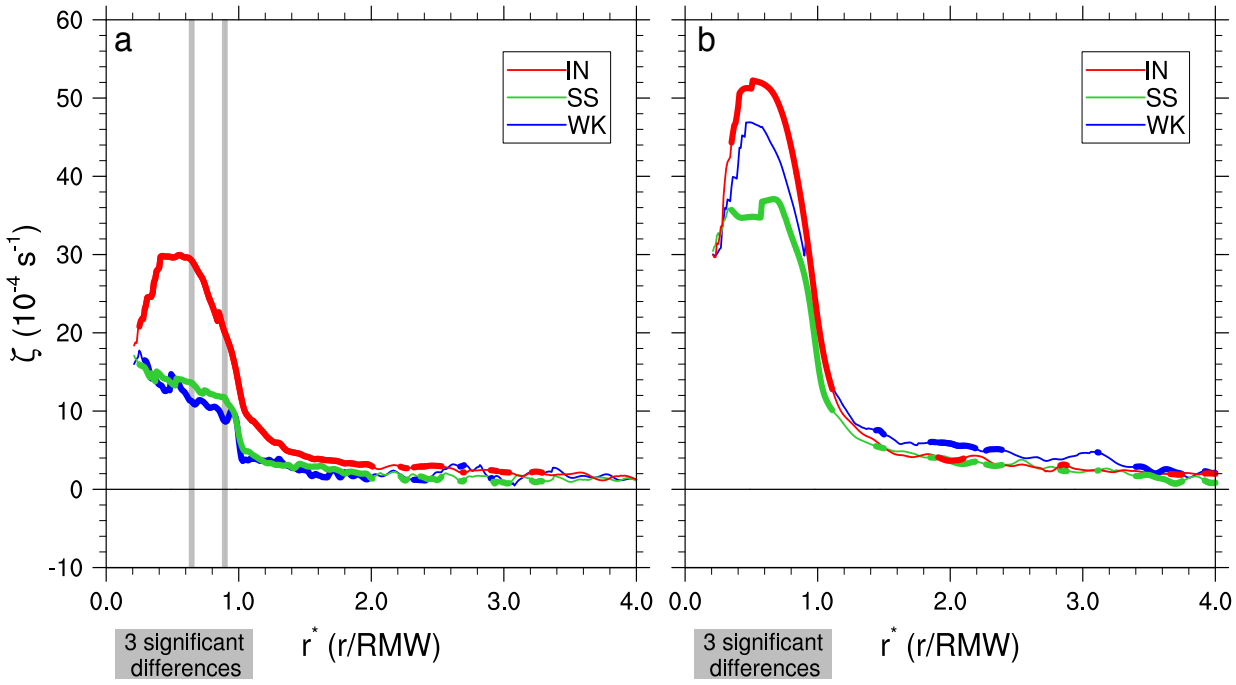

Figure 3.3: As in Figure 3.1, but for axisymmetric vertical vorticity.

3.4 Inertial stability

Axisymmetric inertial stability was calculated using the axisymmetric vertical vorticity mentioned above and the angular velocity calculated from the smoothed azimuthal mean storm-relative axisymmetric tangential wind. The formula is given by

$$I^2 = (f + \zeta)(f + \frac{2\bar{V}}{r}) \tag{3.2}$$

where ζ is the axisymmetric vertical vorticity computed from the smoothed azimuthal mean storm-relative axisymmetric tangential wind velocity ($\bar{V}$), f is the Coriolis parameter evaluated for a given flight, and r is the radial distance. The inertial stability composite-means are shown in Figure 3.4. It is obvious from these results that the inertial stability profiles in all hurricanes and major hurricanes are quite similar to their constituent vorticity profiles.

There is a ring-like structure of inertial stability in the eye of IN hurricanes and major hurricanes, as well as WK major hurricanes. Furthermore, IN hurricanes possessed higher inner and outer-core inertial stability compared to SS and WK hurricanes although the magnitude of these differences were small compared to those found in the eye. Specifically, IN hurricanes possessed anywhere between 2–6$\times 10^{-6}$ s^{-2} more inertial stability in the eye compared to WK or SS hurricanes whereas differences in the inner and outer-core were often less than 1×10^{-6} s^{-2} with a maximum difference of $\sim 6 \times 10^{-6}$ s^{-2} near $r^* = 0.8$. IN major hurricanes possessed significantly higher inertial stability in the eye and inner-core compared to SS major hurricanes with statistically significant differences ranging between 10–16$\times 10^{-6}$ s^{-2} in the eye and 1–15$\times 10^{-6}$ s^{-2} in the inner-core. Overall, major hurricanes possessed anywhere between 2–8 times more inertial stability inside the RMW compared to hurricanes for each respective intensity change bin, demonstrating that the eye and inner-core region of major hurricanes is much more inertially resistant compared to hurricanes.

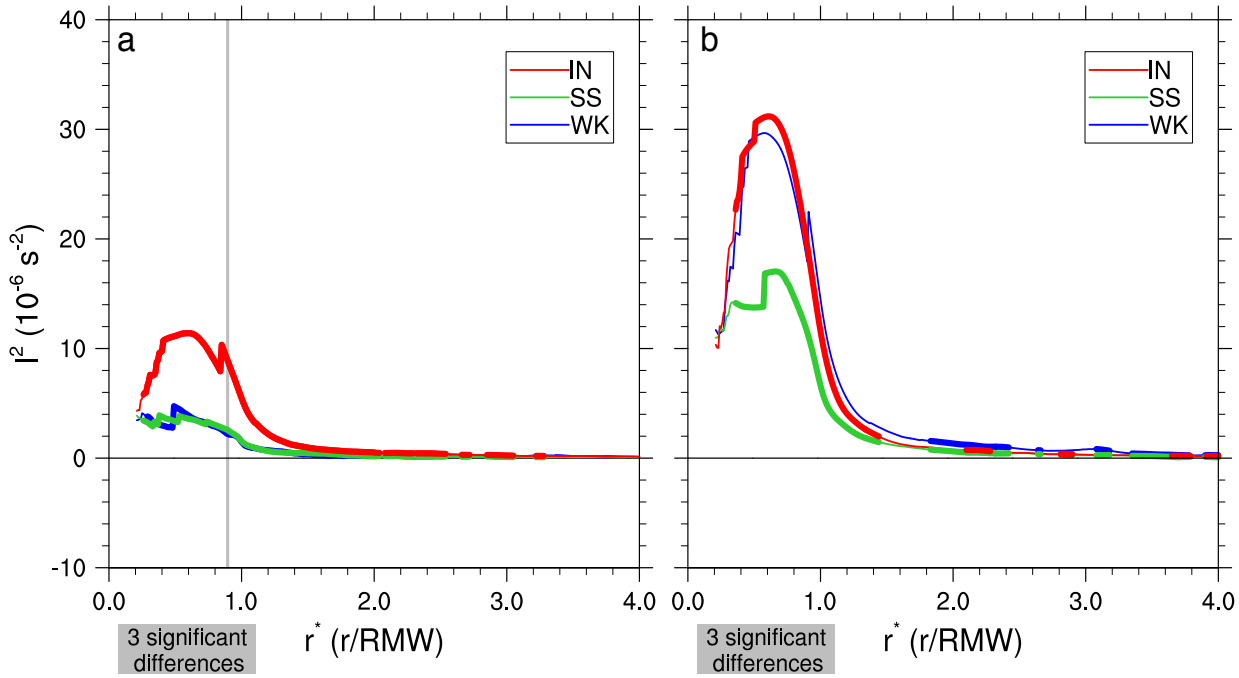

Figure 3.4: As in Figure 3.1, but for axisymmetric inertial stability.

3.5 Absolute angular momentum

The axisymmetric absolute angular momentum was calculated from the smoothed azimuthal mean storm-relative axisymmetric tangential wind and is given by

$$M = r\bar{V} + \frac{fr^2}{2} \tag{3.3}$$

where $\bar{V}$ is the smoothed azimuthal mean storm-relative axisymmetric tangential wind velocity, f is the Coriolis parameter evaluated for a given flight, and r is the radial distance. The results for the absolute angular momentum composite-mean profiles presented large variability within each bin due its strong radial dependence. Therefore, the absolute angular momentum was normalized by its value at the RMW prior to computing the composite-means. The non-dimensional absolute angular momentum profiles were then composited for each bin and these results are presented in Figure 3.5 where M^* represents the non-dimensional absolute angular momentum. These results are generally consistent with what we would expect given the tangential wind velocity composite-means in Figure 3.1. IN hurricanes exhibited the lowest absolute angular momentum inside the eye, followed by SS and then WK hurricanes. Major hurricanes exhibited slightly less variability in the eye although the differences were statistically significant at the 5% level. Overall, IN TCs were characteristic of the lowest absolute angular momentum in the outer-core region.

The dimensional M composite-means revealed that in all cases, IN TCs had physically lower absolute angular momentum at essentially all radii (Figure 3.6). The jagged shapes of the dimensional M composite-means demonstrate the effects of a strong radial dependence and they also highlight that data from individual azimuthal means composing the composite-mean are likely ending at different radii, causing the composite-mean to jump. Further evidence to support this statement is given by the SS and WK hurricane composite-means which show an overall trend of decreasing M outside $r^* = 2.6$. M should only increase with increasing radius for an inertially stable vortex. The observed decrease in M outside $r^* = 2.6$ for SS and WK hurricanes is due to data ending at different radii, causing the composite-mean to jump to different values that represent the "average" M. IN hurricanes were found to possess anywhere between 2–3 times less (dimensional) absolute angular momentum compared to SS and WK hurricanes, which was statistically significant at the 5% level. Statistically significant differences between IN and SS major hurricanes were weaker in magnitude compared to the differences observed between hurricanes, with SS major hurricanes possessing between 10–140$\times 10^4$ m^2 s^{-1} higher absolute angular momentum.

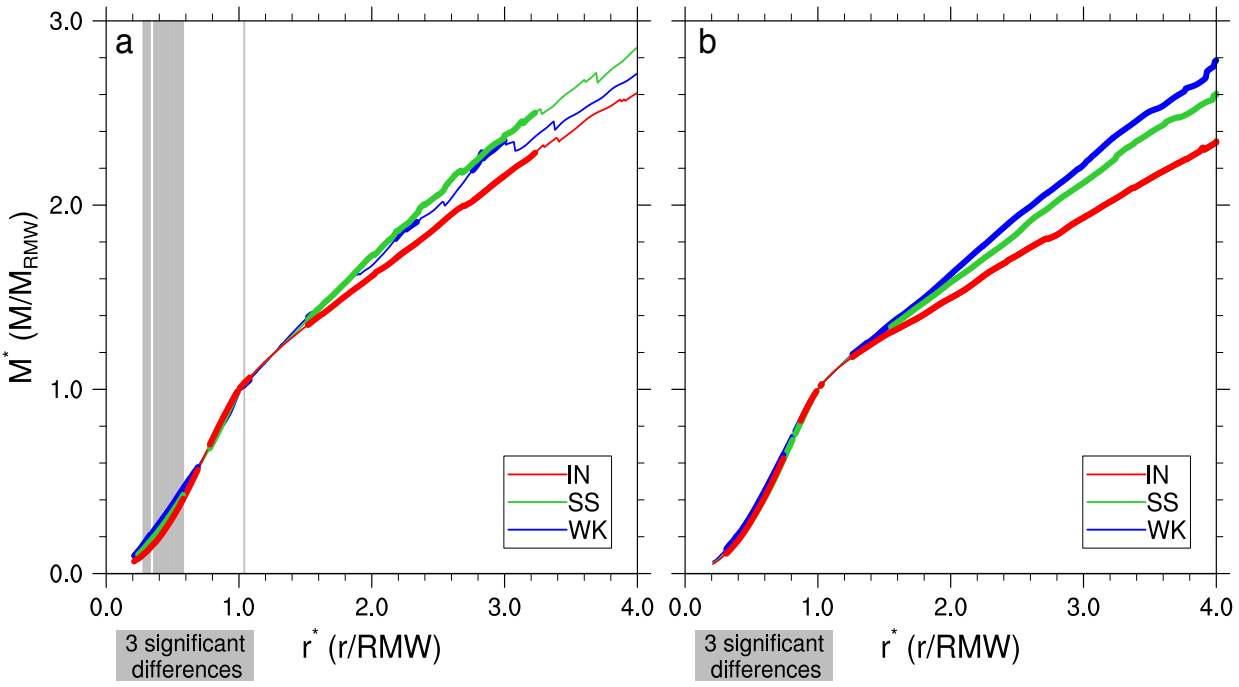

Figure 3.5: As in Figure 3.1, but for non-dimensional absolute angular momentum.

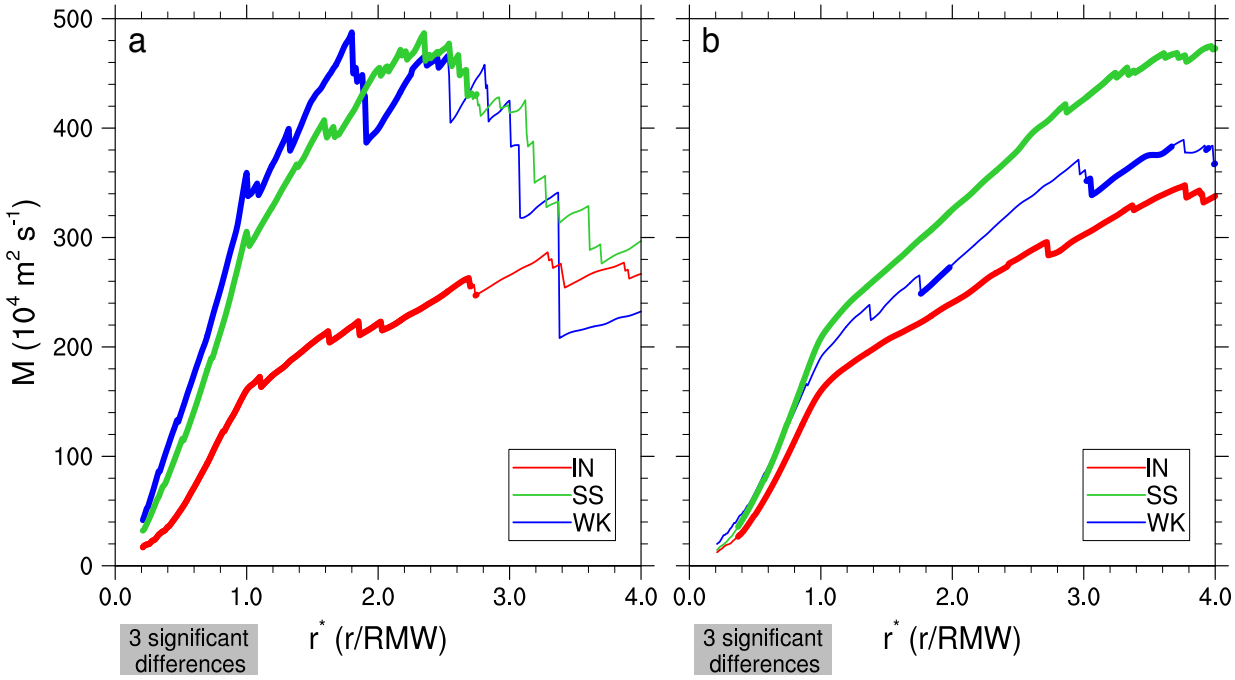

Figure 3.6: As in Figure 3.1, but for dimensional absolute angular momentum.

CHAPTER 4
THERMODYNAMIC COMPOSITE-MEAN STRUCTURES

4.1 Temperature

The thermodynamic composite-means were constructed with the same methodology as the kinematic composite-means. The results for the composite-mean temperature structures are shown in Figure 4.1 and in general demonstrate minor differences for both hurricanes and major hurricanes. IN hurricanes had warmer eyes compared to SS or WK hurricanes. The magnitude of the statistically significant differences between IN and WK hurricanes in the eye were on the order of 1 K. On the other hand, WK major hurricanes possessed warmer temperatures in the inner and outer-core regions compared to IN and SS major hurricanes, with statistically significant differences on the order of 1 K as well. These results suggest that the temperature characteristics of major hurricanes are distinct from hurricanes for a given intensity change.

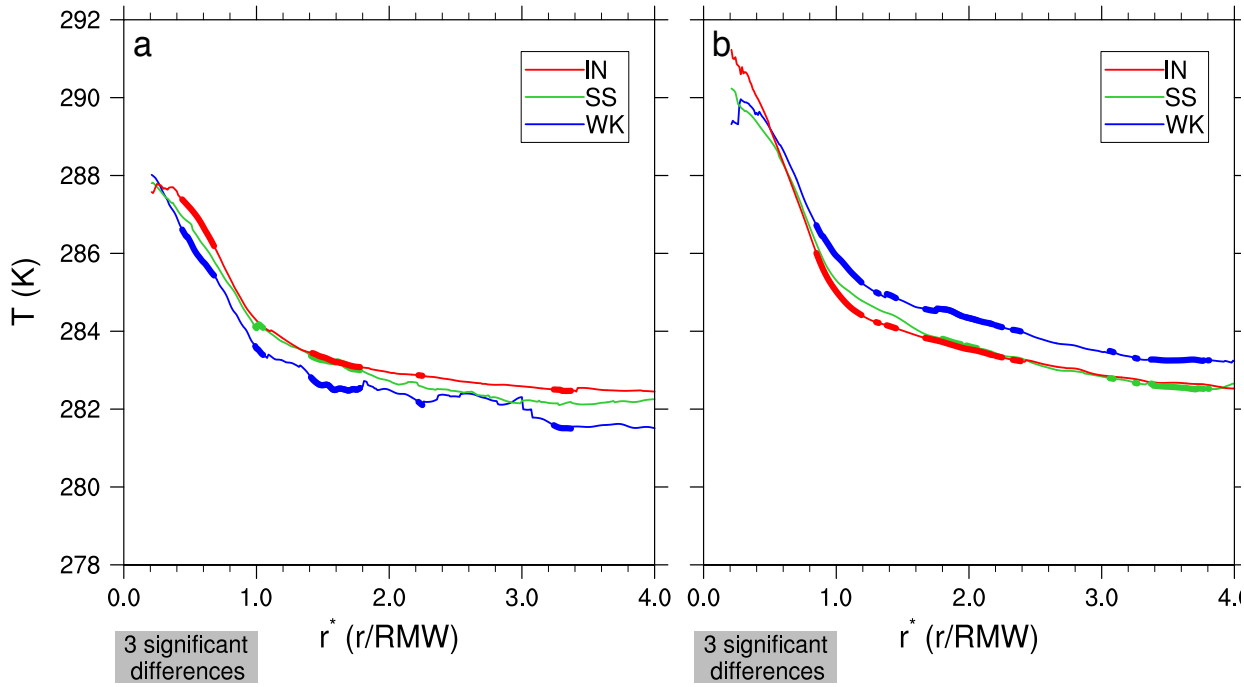

Figure 4.1: As in Figure 3.1, but for temperature.

4.2 Dewpoint temperature

Figure 4.2 illustrates the composite-mean structures of dewpoint temperature. IN hurricanes possessed the highest dewpoint temperatures compared to both SS and WK hurricanes beginning in the eye, with statistically significant differences in the inner and outer-core. The magnitude of the statistically significant differences ranged from 1–2 K in the inner and outer-core regions. Major hurricane composite-mean structures of dewpoint temperature exhibited less differences at all radii compared to hurricanes. IN major hurricanes possessed lower dewpoint temperatures in the eye compared to both SS and WK major hurricanes, statistically significant at the 5% level, suggesting that IN major hurricanes have drier eyes compared to SS and WK major hurricanes.

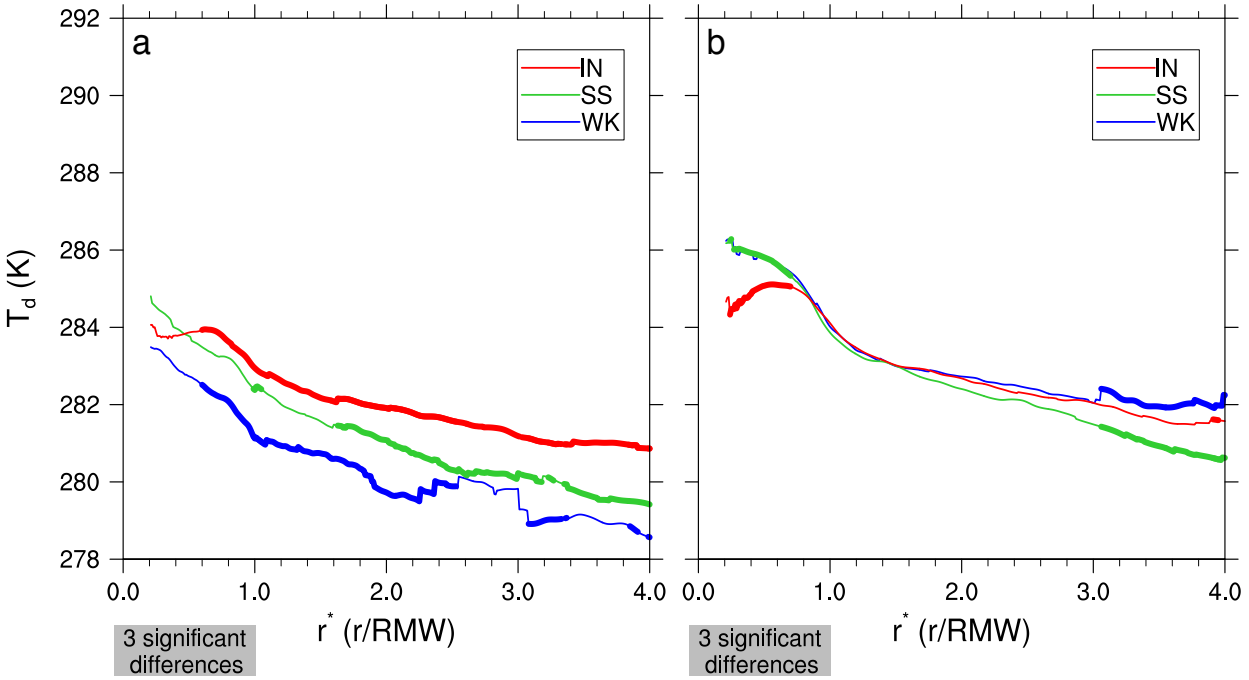

Figure 4.2: As in Figure 3.1, but for dewpoint temperature.

4.3 Dewpoint depression

Results from temperature and dewpoint temperature composite-means were combined to create composite-mean structures of dewpoint depression, illustrated in Figure 4.3. Dewpoint depression composite-means for TCs (both hurricanes and major hurricanes) demonstrate an interesting result: IN TCs possess higher inner and outer-core moisture compared to SS

or WK TCs, significant at the 5% level. This higher moisture content is considered relative to the temperature composite-means shown in Figure 4.1 and is thus a relative humidity rather than an absolute humidity as denoted by the dewpoint temperature composite-means shown in Figuer 4.2. Statistically significant differences in the inner and outer-core dewpoint depression were between 1–3 K and 1–2 K for hurricanes and major hurricanes, respectively. Moisture content in this region was found to play an important role in distinguishing the intensity change phase of a TC. IN major hurricanes were also found to have drier eyes compared to SS or WK major hurricanes as shown in Figure 4.2. Specifically, IN major hurricanes possessed an ∼1–2.5 K higher dewpoint depression than SS major hurricanes, statistically significant at the 5% level. An emphasis is placed on the higher moisture content in the inner and outer-core region due to its robust signal in both hurricanes and major hurricanes.

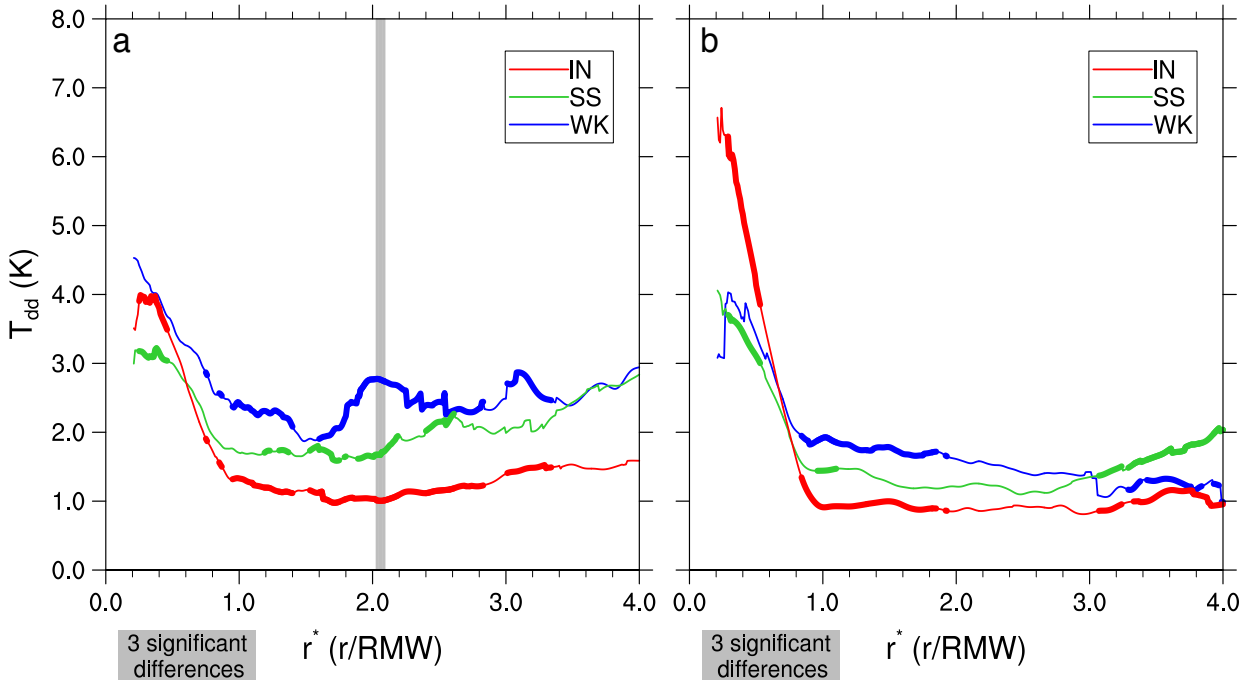

Figure 4.3: As in Figure 3.1, but for dewpoint depression.

4.4 Equivalent potential temperature

Equivalent potential temperature (θ_e) composite-means were also created using the same compositing methodology and are shown in Figure 4.4. Calculation of θ_e followed the empir-

ical formulas derived by Bolton (1980). The higher temperature and dewpoint temperatures for IN hurricanes at nearly all radii contributed to higher θ_e when compared to the SS and WK hurricanes. Statistically significant differences between IN and SS hurricanes ranged from 1–2 K while statistically significant differences between IN and WK hurricanes were on the order of ∼3 K. In contrast to the hurricanes, there were minimal differences amongst the major hurricane θ_e composite-means. The WK major hurricanes generally had the highest θ_e compared to SS and IN major hurricanes, but these results were generally not statistically significant aside from WK major hurricanes possessing ∼4 K higher θ_e than SS major hurricanes between $r^* = 3$–4.

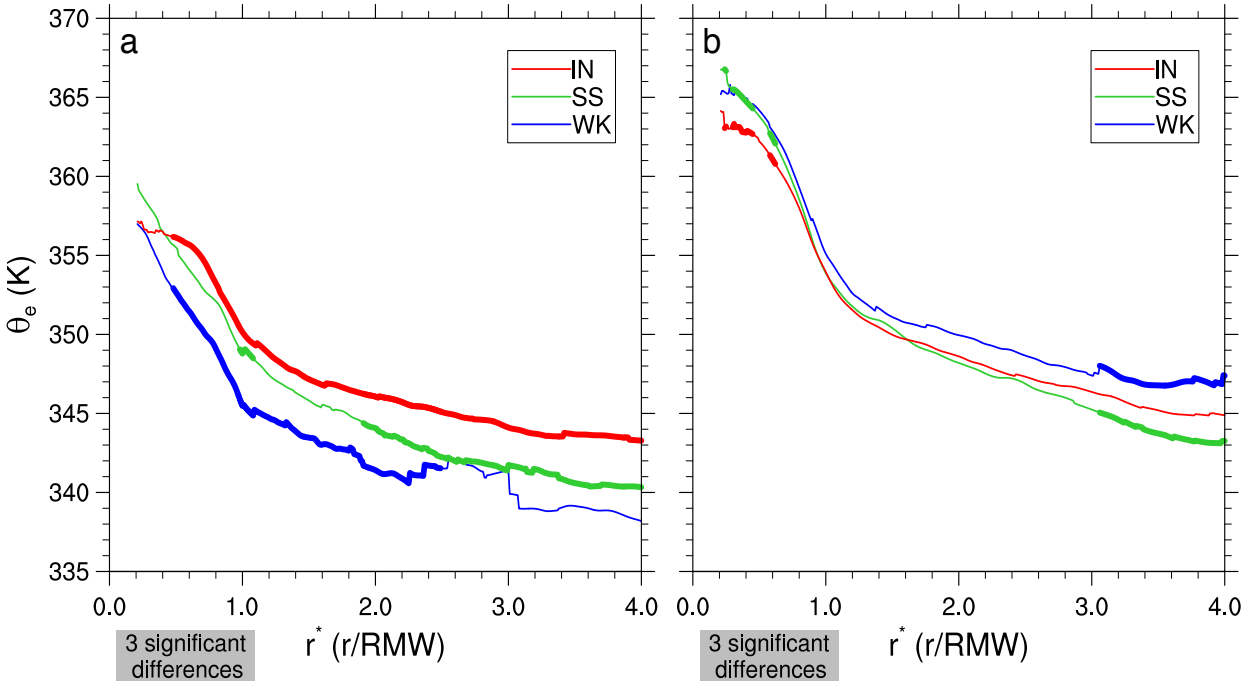

Figure 4.4: As in Figure 3.1, but for equivalent potential temperature.

CHAPTER 5
DISCUSSION

5.1 Gradients of tangential wind

Differences in the tangential wind velocity gradients inside and outside the RMW have been documented by several flight level studies in the past. The results presented in this study are consistent with those presented by both Willoughby (1990) and Kossin and Eastin (2001) and it is speculated that both the presence (or absence) of a strong convective ring and radial mixing are likely influencing the observed tangential wind gradient differences between WK, SS, and IN TCs. Elevated tangential flow in the eye of WK and SS TCs (Figure 3.1) support the idea of flow across the eye and eyewall leading to solid body rotation proposed by Kossin and Eastin (2001). This is further supported by higher absolute angular momentum in the eye of SS and WK TCs (Figure 3.5). Differences in the tangential wind and absolute angular momentum in the eye between hurricanes were much larger than those observed between major hurricanes, possibly suggesting that the presence of significantly higher inertial stability inside the RMW for major hurricanes (Figure 3.4) is preventing structural differences caused by inward radial advection for all intensity changes. The steep tangential wind gradients of IN hurricanes and major hurricanes, coupled with a vorticity ring structure, supports the presence of a strong convective ring as observed by Willoughby (1990). It's interesting to note that the tangential wind differences were greatest inside the RMW for hurricanes and outside the RMW for major hurricanes. These results further support the statement that the eye of hurricanes may be more susceptible to changes caused by radial mixing near the eye and eyewall when compared to major hurricanes.

Results were further stratified by TC age as described in section 2.5. Figure 5.1 illustrates the composite-mean tangential wind velocity structures for early and late stage hurricanes and major hurricanes, and reveals that the observed tangential wind velocity gradient differences between hurricanes in the eye were more pronounced during the later stages of their life cycle. This result suggests that strong convective rings may be present for IN hurricanes regardless of their age and that the relaxation of tangential flow across the eye may occur preferentially during the later stages of the life cycle for WK and SS hurricanes. However, the early stage tangential wind structure differences in the eye show a similar pattern. The results may have lost their statistical significance due to the fact that the sample sizes have

also decreased. On the other hand, the outer-core tangential wind gradient structural differences observed for major hurricanes occurred primarily during the early stages of their life cycle, suggesting that the outer-core structure of major hurricanes may be more susceptible to changes from physical processes occurring during early stages of their life cycle. The aforementioned tangential wind structural differences were observed regardless of the intensity change time (i.e., previous, centered, or future) utilized to bin the data (Figure 5.2). Therefore, the physical processes attributed to causing the observed structural differences may be present throughout a 24 h intensity change window. One notable exception would be the reduction of tangential wind velocity near the RMW for WK major hurricanes during the late stage of their life cycles, suggesting that once weakening has begun, it will continue into the later stages.

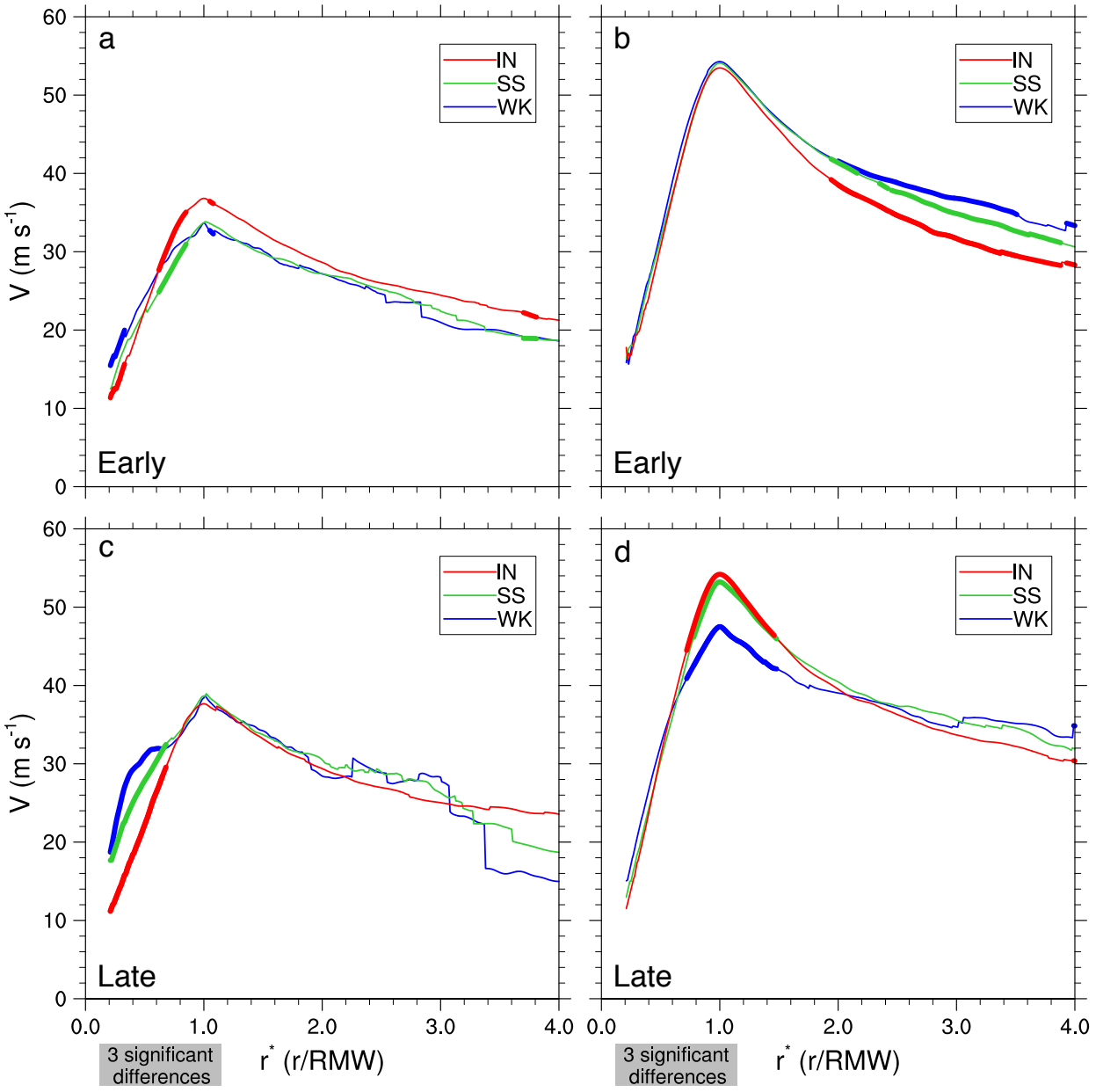

Figure 5.1: Storm-relative axisymmetric tangential wind velocity composite-means for early stage hurricanes (a) and major hurricanes (b), and late stage hurricanes (c) and major hurricanes (d). Radial locations where all composite-means were significantly different at the 5% level are shaded in gray and two significantly different composite-means are denoted in bold.

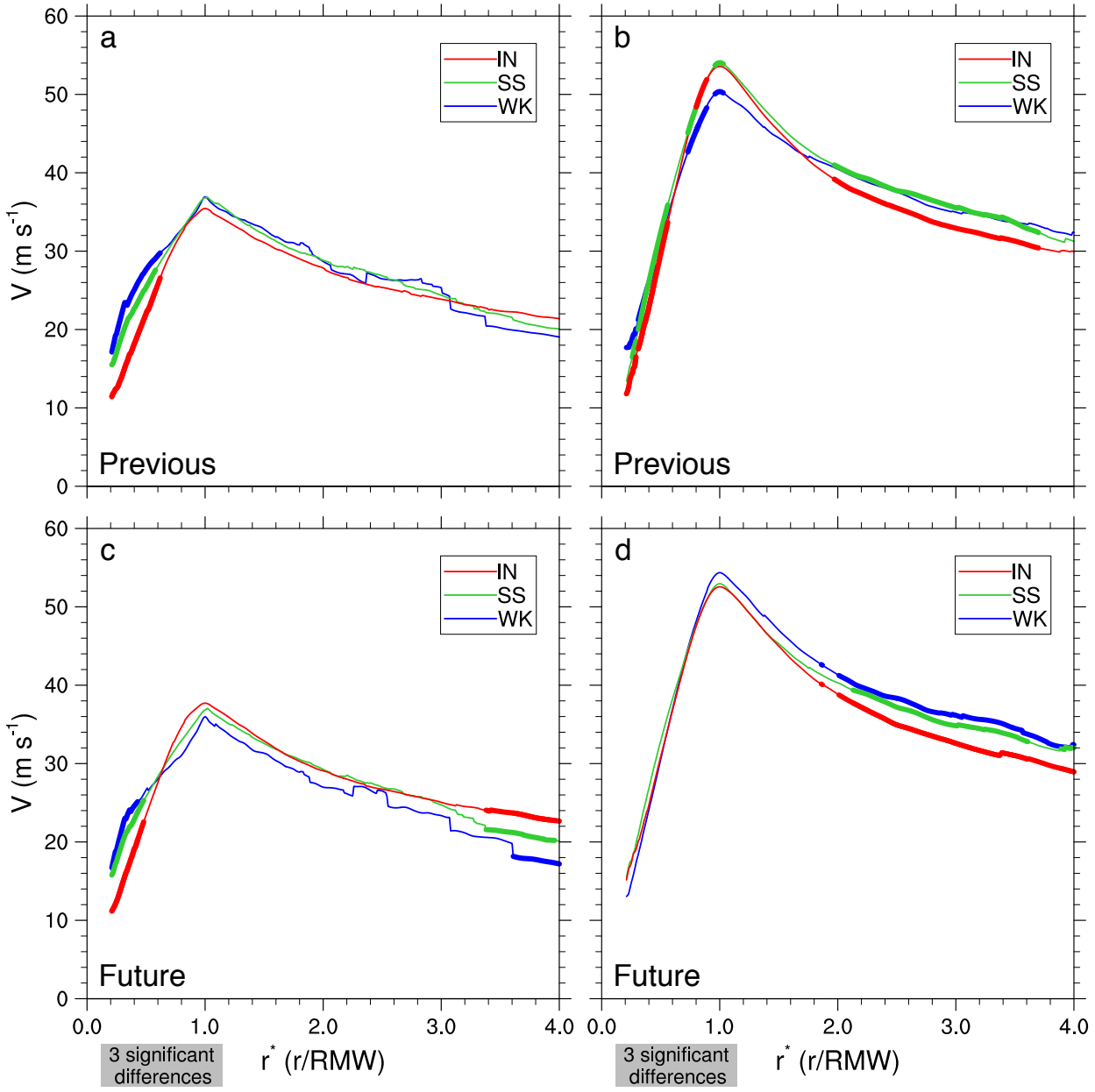

Figure 5.2: Storm-relative axisymmetric tangential wind velocity composite-means for hurricanes and major hurricanes using a previous 12 h intensity change (a and b, respectively) and hurricanes and major hurricanes using a future 12 h intensity change (c and d, respectively). Radial locations where all composite-means were significantly different at the 5% level are shaded in gray and two significantly different composite-means are denoted in bold.

5.2 Vorticity ring structure and outer-core vorticity

The one-dimensional nature of the flight level data prevented an examination of PV, however the vertical vorticity can be used as a proxy for PV as done by Kossin and Eastin (2001) and Mallen et al. (2005) in relation to the PV ring discussed by Schubert et al. (1999). Figure 5.3 further illustrates that IN TCs possess a vorticity ring structure regardless of their age, suggesting that a vorticity ring, likely associated with the presence of a strong convective ring, is an inherent feature of IN TCs. Rogers et al. (2013) and Rogers et al. (2015) demonstrated that for an IN TC, convective bursts (CBs) were primarily located inside the RMW, collocated with the vorticity ring, which would maximize the efficiency of diabatic heating produced by the CBs (Vigh and Schubert 2009). Although the flight level data utilized in this study precludes the observation of CBs, the similarities of our results with those presented by Rogers et al. suggest that these features may be contributing to the vorticity ring through vortex tube stretching enhanced by low-level convergence in that region. It should be noted that CBs were found to have time scales on the order of one to three hours (Rogers et al. 2015) so it's difficult to fully attribute the observed features in the results to CBs. In general, the results demonstrate that a ring of intense convection was likely present for IN TCs. In the case of WK major hurricanes, the vorticity ring may have been formed through similar processes prior to the system reaching its weakening state. This statement is supported by the results presented in Figure 5.4d when considering a future 12 h intensity change as opposed to a centered 12 h intensity change. Major hurricanes that will weaken in the next 12 hours are shown to possess a vorticity ring structure, thus verifying that there must be similar processes contributing to this feature leading up to the breakdown of the vorticity ring and weakening state of the system. In the case of SS major hurricanes, the flat vorticity profile inside the RMW is indicative of a transition to a more monotonic profile of vorticity associated with the breakdown of the vorticity ring (Schubert et al. 1999).

WK major hurricanes possessed higher outer-core vorticity and inertial stability compared to SS and IN major hurricanes. In contrast, outer-core vorticity and inertial stability for IN hurricanes were highest when compared to SS or WK hurricanes. The results derived for hurricanes contrast those presented by Rogers et al. (2013) who found higher outer-core vorticity for SS TCs compared to IN TCs. Furthermore, SS major hurricanes were found to have no statistically significant differences in vorticity and inertial stability when compared to IN major hurricanes, another result which contrasts those presented by Rogers et al. (2013). Discrepancies between the results presented in this study and those presented by Rogers

et al. (2013) may have risen from the different methods by which vorticity was calculated, the different sample sizes, and different stratification methods. Rogers et al. (2013) computed the axisymmetric vertical vorticity for each radial pass on a Cartesian grid (i.e., $\zeta = \partial v/\partial x - \partial u/\partial y$), converted to cylindrical coordinates, azimuthally averaged, and then created the composite-means. In this study, axisymmetric vertical vorticity was calculated (in cylindrical coordinates) from the smoothed azimuthal mean storm-relative tangential wind profiles and then the composite-mean vorticity was computed for each bin. Here, we additionally explore physical processes that may contribute to the observed discrepancies.

The elevated outer-core vorticity associated with WK major hurricanes (Figure 3.3b) is consistent with the broader tangential wind field that was observed in Figure 3.1b. Broadening of the tangential wind field is often regarded as a feature that develops with increasing age. Figure 5.1b illustrates that a broadening of the tangential wind field in major hurricanes may be observed to cause structural differences between WK, SS, and IN major hurricanes at early stages in their life cycles. Table 5.1 reveals that SS and WK hurricanes, on average, were the oldest of all TCs in the analysis. However, hurricanes exhibited much less tangential wind velocity differences in the outer-core compared to major hurricanes. Therefore, the effects of broadening possibly increasing outer-core tangential winds for WK and SS TCs is speculated to have its strongest influence at major hurricane intensity.

Broadening of the tangential wind field is also often associated with the formation of a concentric eyewall (Sitkowski et al. 2011; Willoughby et al. 1982; Willoughby 1990) which eventually leads to a flat tangential wind structure outside the RMW. It is speculated that concentric eyewalls may have an impact on the composite tangential wind field for WK and SS major hurricanes in the results presented. Furthermore, a secondary wind maximum replacing the inner wind maximum effectively increases the RMW, causing the wind structure found inside the RMW to be quite different when normalizing the radius coordinate by the RMW. Future efforts will include an objective determination and removal of concentric eyewall cases to determine if they are primary or secondary contributors to the observed structural differences in the outer-core region. For the purpose of this study, the presence of secondary eyewalls in the composites is a possibility since we have not isolated these cases.

Combining the results observed for tangential wind velocity and vorticity when further stratifying by TC age (Figures 5.1 and 5.3) highlights a significant change in the tangential wind velocity and vorticity structure for WK major hurricanes. At early stages, WK major hurricanes possessed a strong vorticity ring structure with a composite-mean peak vorticity value greater than that observed for IN major hurricanes. During the late stage, the

Table 5.1: Composite-mean flight age and normalized flight age for each intensity and centered 12 h intensity change bin. Standard deviations are given in parentheses. See section 2.5 for a description on how the normalized flight age was computed.

Bin	Age (days)	Normalized Age
Hurricanes		
WK	7.28 (2.74)	0.67 (0.17)
SS	6.78 (3.19)	0.64 (0.18)
IN	4.74 (2.69)	0.49 (0.22)
Major Hurricanes		
WK	6.81 (2.44)	0.60 (0.14)
SS	6.72 (2.17)	0.55 (0.12)
IN	5.37 (2.15)	0.49 (0.16)

vorticity ring completely vanished and WK major hurricanes transitioned to a monotonic profile of vorticity inside the RMW. Coupled with this monotonic profile of vorticity was a decrease in the maximum tangential wind velocity, a decrease in the outer-core tangential wind velocity, and an overall flatter outer-core tangential wind structure (Figure 5.1d). Inertial stability composite-mean structures followed suit with the changes observed for vorticity when considering TC age. These features highlight the significance of considering TC age when observing the kinematic structure of major hurricanes.

Contrary to the results presented for major hurricanes, IN hurricanes had the highest outer-core vorticity compared to SS and WK hurricanes, paired with higher inner-core vorticity associated with the vorticity ring structure. Comparing the early and late stage vorticity profiles for IN hurricanes (Figures 5.3a,c) reveals that the magnitude of outer-core vorticity did not vary much. Instead, the outer-core vorticity of WK and SS hurricanes is observed to decrease during the later stages of their life cycles. Therefore, it is speculated that since WK and SS hurricanes are closer to the end of their life cycles (cf. Table 5.1), they may have already experienced their maximum intensity and will not undergo reintensification. Convective activity in the outer-core region is speculated to have diminished or weakened significantly for WK and SS hurricanes compared to IN hurricanes, contributing to weaker values of vorticity in this region.

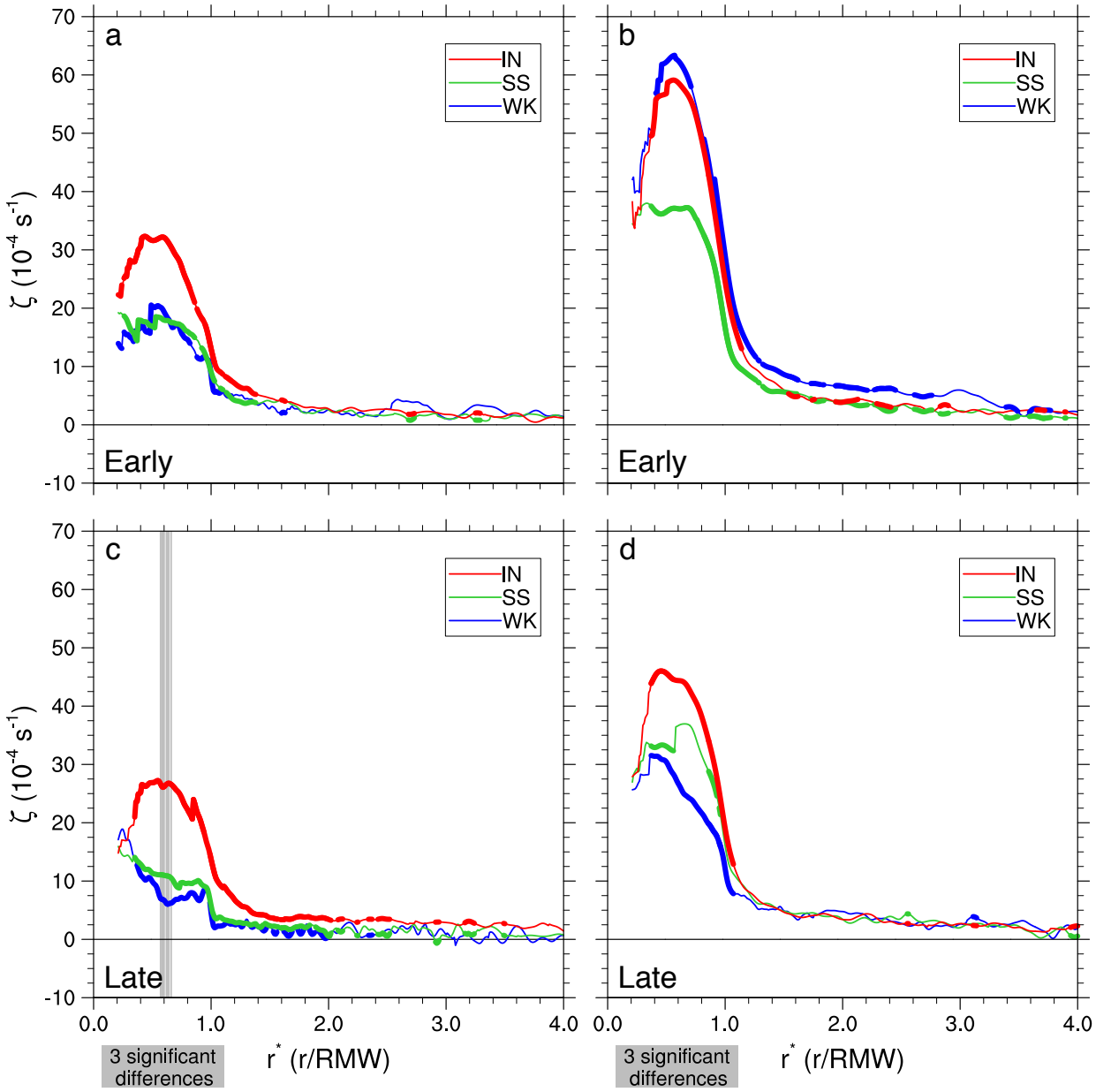

Figure 5.3: As in Figure 5.1, but for axisymmetric vertical vorticity.

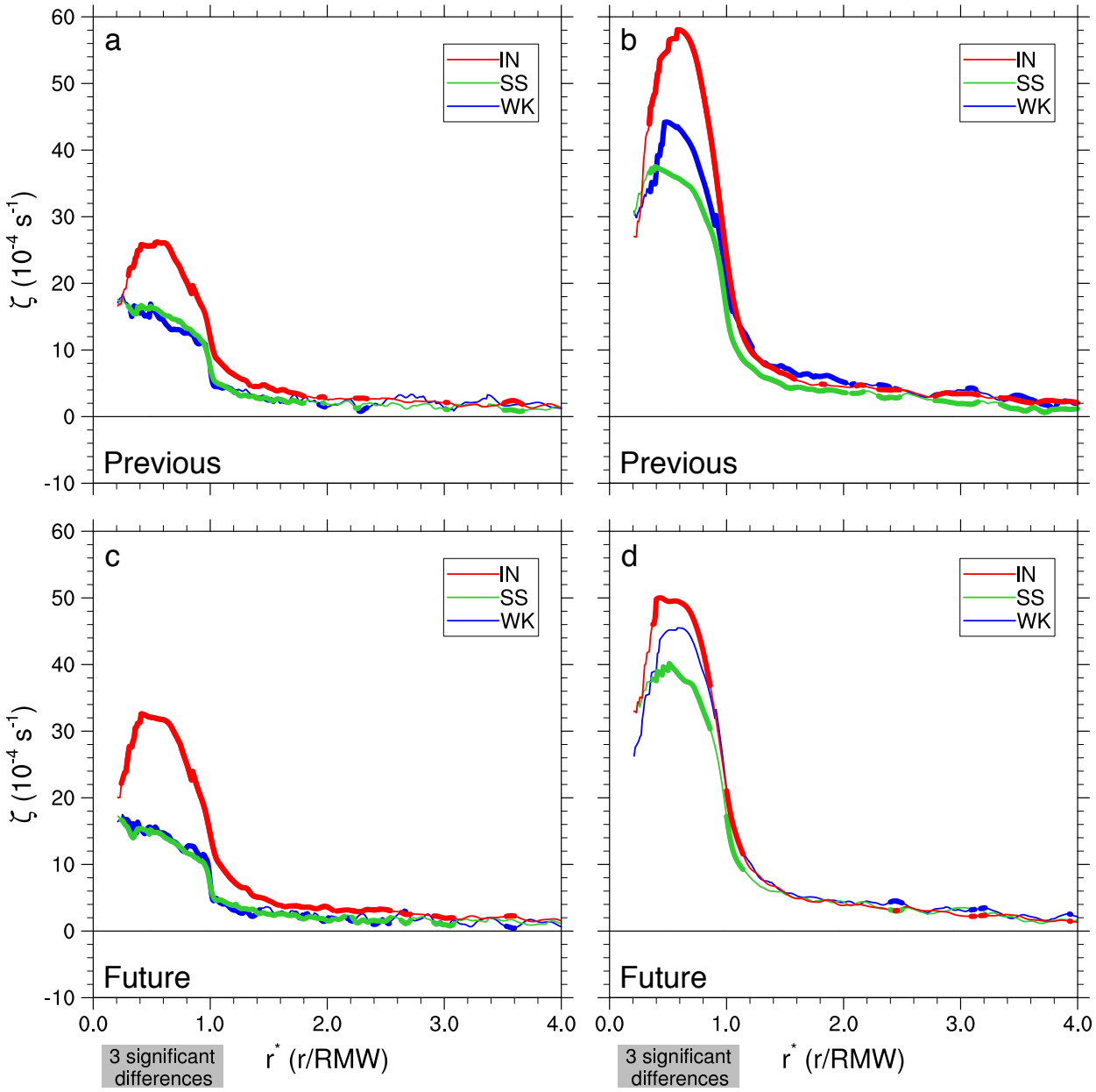

Figure 5.4: As in Figure 5.2, but for axisymmetric vertical vorticity.

5.3 Absolute angular momentum

Results derived for absolute angular momentum revealed that IN TCs possessed the (physically) lowest absolute angular momentum at all radii. The non-dimensional analysis showed IN TCs having weaker absolute angular momentum in the eye and in the outer-core

region relative to SS and WK TCs. Since absolute angular momentum can be partitioned in to storm and earth relative contributions[1], the results beg the question: are IN TCs characterized by lower angular momentum or are they located in regions where Earth's angular momentum is lower? Assessing this question requires analyzing the two contributions to absolute angular momentum independently. Angular momentum contributions from the storm can be given in cylindrical coordinates by

$$M_s = r\bar{V} \tag{5.1}$$

where $\bar{V}$ represents the smoothed azimuthal mean storm-relative axisymmetric tangential wind velocity. Angular momentum contributions from Earth are then given by

$$M_e = fr^2/2. \tag{5.2}$$

Rather than creating composite-mean structures of M_s and M_e, we offer a discussion that suffices for their contributions. As observed in the composite-mean tangential wind velocity results (Figure 3.1) and discussed earlier, WK and SS major hurricanes possess a broader circulation outside the RMW compared to IN major hurricanes. This broader circulation serves to increase the angular momentum directly through higher local tangential wind velocities. In these regards, the WK and SS major hurricanes can possess higher outer-core angular momentum solely from contributions due to the storm. Additionally, absolute angular momentum in the eye was higher for WK and SS TCs compared to IN TCs; a feature which was attributed to the possible relaxation of flow across the eyewall as observed by Kossin and Eastin (2001). Therefore, the observed angular momentum differences at all radii can be explained from contributions due to storm-scale differences.

Considering the contributions from Earth's angular momentum, WK and SS TCs are often found at higher latitudes than IN TCs. This statement holds true for the results presented in this analysis, as can be seen in Table (5.2) which shows the average Coriolis parameter for each bin in the furthest right column. WK and SS TCs are located in regions that are influenced by a stronger Coriolis force (higher latitudes) compared to IN TCs. These differences were statistically significant at the 5% level when comparing SS and WK hurricanes to IN hurricanes using the two-tailed WMW rank-sum test, however no statistically significant differences were found between major hurricanes. Therefore, it is speculated that

[1]Storm and Earth relative contributions are referred to as contributions from the storm's tangential wind field and Earth's angular momentum, respectively.

both contributions relative to the storm and Earth are relevant to causing lower absolute angular momentum at all radii for IN TCs. Furthermore, since M is strongly dependednt on radius, the varying RMW sizes shown in Figure 2.3 suggest that differences in the size of the RMW for each composite may also signiciantly contribute to the observed differences in M.

5.4 Thermodynamic structural differences

Thermodynamic structures revealed that IN TCs possessed higher moisture content in the outer-core region compared to SS or WK TCs (cf. Figure 4.3). In the case of IN hurricanes, warmer temperatures and higher dewpoint temperatures contributed to higher θ_e relative to SS and WK hurricanes at nearly all radii. Kossin and Eastin (2001) found that regime 1 TCs were characteristic of elevated θ_e in the eyewall and regime 2 TCs transitioned to a monotonic profile of θ_e, with maximum θ_e in the eye. Although the results for IN hurricanes do not necessarily indicate elevated θ_e near the eyewall, SS and WK hurricanes were characteristic of a monotonic θ_e profile. Elevated vorticity near the eyewall for IN hurricanes would be consistent with the previously presented idea that strong convective rings are likely present for IN hurricanes, however, thermodynamic evidence of a strong convective ring structure is not apparent in the results presented. This does not rule out the possibility that strong convective rings are present for IN hurricanes, but rather it suggests that the thermodynamic signature is not as strong as the kinematic signal when considering azimuthally averaged structures. It is speculated that the thermodynamic features contributing to the different structures observed by Kossin and Eastin (2001) evolved on time scales that were too short to be resolved after azimuthal averaging and compositing. As mentioned earlier, the time scale of CBs is on the order of one to three hours. It is likely that the thermodynamic features observed for regime 1 TCs by Kossin and Eastin (2001) are caused by the presence of CBs. The degree to which the moisture content for hurricanes was impacted by the large scale environment also comes to question. Table 5.2 shows that IN hurricanes had the highest relative humidity (RH; see section 2.3 for SHIPS variable descriptions) followed by SS and then WK hurricanes. These differences in large scale RH were statistically significant at the 5% level when comparing WK hurricanes to IN or SS hurricanes. Therefore, it is speculated that the large scale moisture environment may have played an important role in contributing to the observed thermodynamic structures in hurricanes, especially in the outer-core region.

Although IN major hurricanes possessed higher outer-core moisture relative to SS and

WK major hurricanes (cf. Figure 4.3), higher temperature found in WK major hurricanes allowed them to possess higher θ_e at nearly all radii. These results sharply contrast those presented for hurricanes and suggest that distinct physical processes may be occurring between hurricanes and major hurricanes that contribute to these differences. It is speculated that WK major hurricanes may have had sufficient time to develop a reservoir of higher θ_e compared to SS or IN major hurricanes. IN major hurricanes also lacked elevated θ_e near the eyewall as was observed for regime 1 TCs in Kossin and Eastin (2001). IN major hurricanes did, however, possess drier eyes compared to WK and SS major hurricanes, suggesting that the degree of adiabatic warming present in the eye may play an important role for distinguishing IN major hurricanes from SS or WK major hurricanes. IN major hurricanes were also observed to have the highest large scale RH compared to WK and SS major hurricanes, but these differences were lesser compared to hurricanes and lacked any statistical significance at the 5% level. Therefore, vortex and/or convective scale processes may be playing a more important role on altering the observed moisture content in major hurricanes compared to hurricanes.

Stratification of the thermodynamic results by age (Figure 5.5) did not reveal any statistically significant differences for hurricanes, suggesting that kinematic processes have a greater contribution to structural differences observed at different stages in the life cycle of a hurricane. Major hurricanes were observed to possess the same moisture content differences at both early and late stages of their life cycle. The lack of any distinct thermodynamic differences when adding the additional consideration of age compared to the results stratified by intensity and intensity change alone suggests that age does not have a significant impact on the thermodynamic structure of TCs within each bin. Figure 5.6 illustrates the dewpoint depression composite-mean structures when considering a previous and future 12 h intensity change. Interestingly, the results suggest that hurricanes exhibit higher variability based on their future intensity change characteristics whereas major hurricanes exhibit higher variability based on their previous intensity change characteristics. Therefore, the thermodynamic structure of a hurricane may likely play a more important role on determining its future intensity change compared to major hurricanes. As mentioned earlier, this result may be due to differences in the large scale characteristics in which a hurricane is located. Regardless of this possibility, the thermodynamic structure of hurricanes may be relevant for forecasting the future intensity change of the system. On the other hand, there were no statistically significant differences in the composite-mean structures of dewpoint depression for major hurricanes when using a future 12 h intensity change. Previous 12 h intensity change results

were similar to those observed for a centered 12 h intensity change, suggesting that these thermodynamic structures were a robust signal throughout the observed time window.

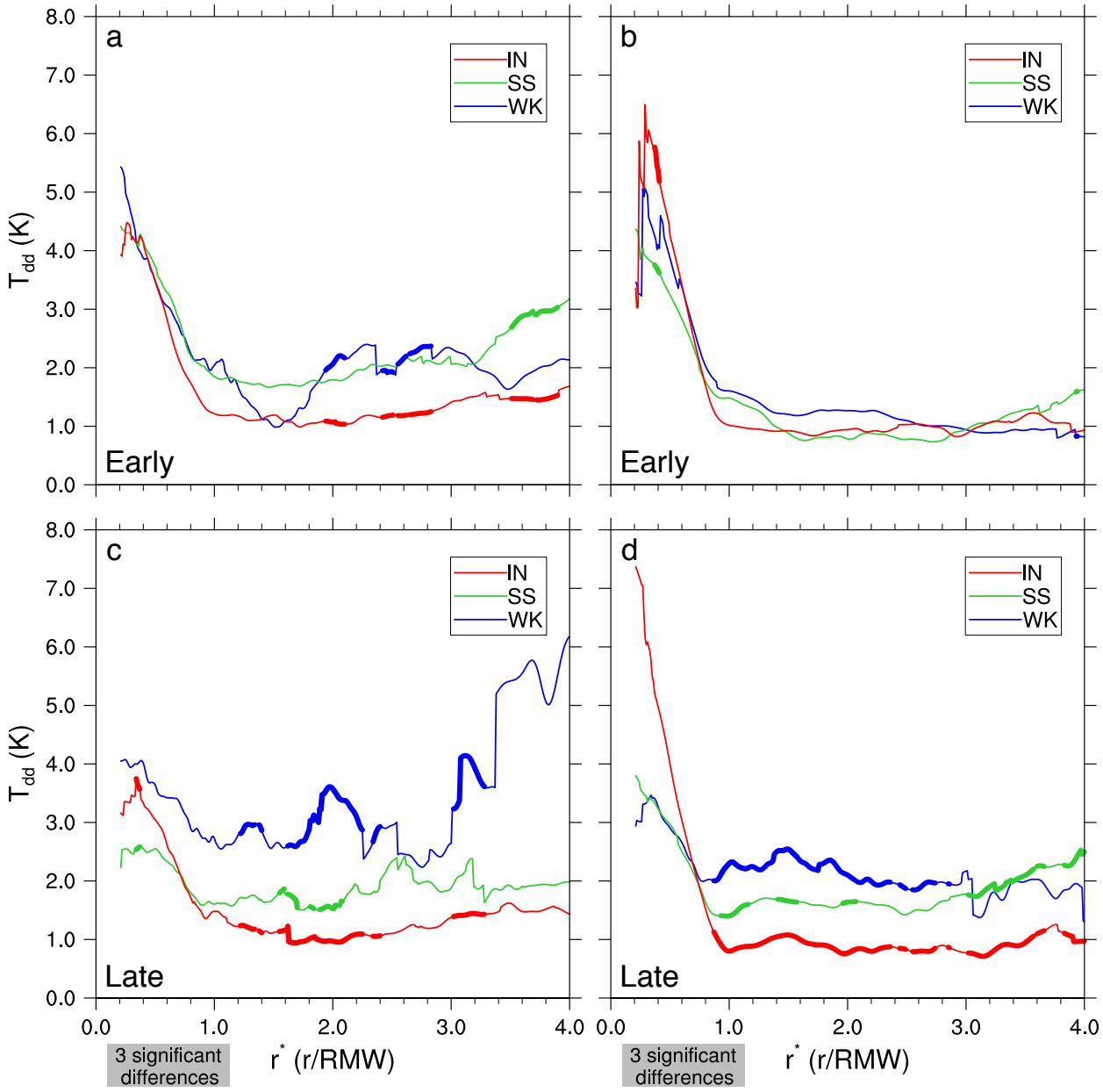

Figure 5.5: As in Figure 5.1, but for dewpoint depression.

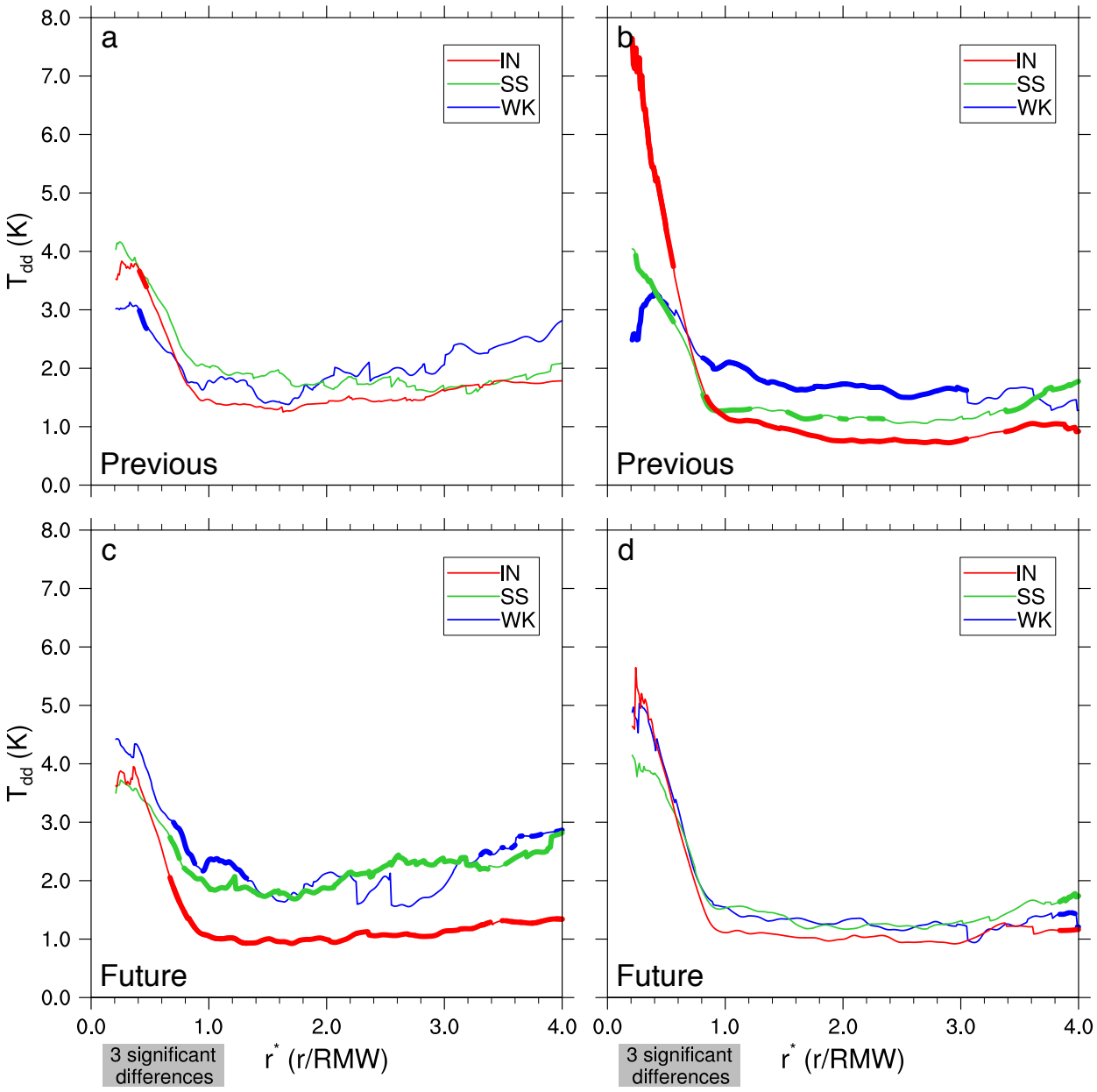

Figure 5.6: As in Figure 5.2, but for dewpoint depression.

5.5 Large scale characteristics

The large scale environment in which TCs exist can play an important role on altering the structure of TCs, which feeds back to altering their intensity change characteristics. In the context of this study, a focus was placed on structural differences that arise due to

the TC's intensity and intensity change rather than the large scale environment in which it was found. Investigation of these large scale characteristics is required to determine if they may have had a significant impact on the observed structural differences shown in chapters 3 and 4. Table 5.2 summarizes the large scale SST, RHLO, SHDC, T200, and f for hurricanes and major hurricanes. In the case of hurricanes, the general trend in the large scale characteristics revealed that IN hurricanes were often located in regions with higher SSTs, higher low-level RH (RHLO), lower VWS averaged from 850–200 mb (SHDC), colder outflow temperatures (T200), and lower Coriolis force (f) compared to SS and WK hurricanes. Many of the observed differences between hurricanes were statistically significant at the 5% level using the two-tailed WMW rank-sum test. Furthermore, SS hurricanes were located in more favorable environments compared to WK hurricanes. On the other hand, no statistically significant differences in the large-scale environment of major hurricanes were observed except for the outflow temperatures of SS and IN major hurricanes.

These combined results imply that hurricanes are more susceptible to structural influences from their large scale environment compared to major hurricanes. Major hurricanes were found to exist in similar environments that are favorable for intensification. They may also be more resilient to changes from their environments due to their well established inner-core and elevated inertial stability as mentioned earlier. This is not to say that the results observed for hurricanes lacked impacts from smaller scale features evolving within the vortex. Rather, it implies that hurricanes may be interacting with more variable large scale environments compared to major hurricanes. In general, the results verify that the composite structures in this study were truly stratified by the internal characteristics of intensity and intensity change rather than just by external large scale characteristics. This is more robust for major hurricanes which were found in similar large scale environments.

Table 5.2: Composite large scale statistics evaluated from the SHIPS database for each bin using a centered 12 h intensity change. The composite-mean value for each bin is given along with the standard deviation in parentheses. Statistically significant differences at the 5% level using a two-tailed WMW rank-sum test are denoted by colored asterisks following the composite-mean value. Colors denote which composite-mean was significantly different from the given composite-mean and color coding follows that used in the composite-mean structure figures (i.e., blue = WK, green = SS, red = IN. For example, a red asterisk next to the composite-mean value of WK SST denotes that it was significantly different from IN SST at the 5% level.

Bin	$RSST(C)$	$RHLO(\%)$	$SHDC(kt)$	$T200(C)$	$f(10^{-5}s^{-1})$
Hurricanes					
WK	28.56* (0.96)	63.52** (7.97)	17.67 (8.88)	-51.01* (1.77)	6.64* (1.40)
SS	28.84 (0.78)	67.30* (6.18)	15.50 (9.06)	-51.17* (1.30)	6.54* (1.10)
IN	29.13* (0.82)	68.70* (8.82)	13.62 (5.82)	-52.17** (1.28)	5.29** (1.30)
Major Hurricanes					
WK	29.04 (0.48)	67.03 (6.22)	10.87 (4.86)	-51.57 (1.24)	5.47 (1.24)
SS	29.07 (0.48)	67.85 (6.10)	11.10 (7.05)	-51.52* (1.04)	5.39 (0.88)
IN	29.04 (0.60)	68.51 (7.69)	9.48 (5.78)	-52.17* (1.13)	5.05 (1.15)

5.6 Statistics evaluated at the RMW

A statistical summary of each kinematic and thermodynamic variable evaluated at the RMW is provided in Tables 5.3 and 5.4, respectively. The average value for each variable is given along with the standard deviation (in parentheses) for all six bins. In addition to the statistics for all of the variables previously discussed, the average (and standard deviation) RMW for each bin is given in the furthest right column of Table 5.3. The average RMW of WK hurricanes was the largest compared to SS and IN hurricanes. A similar pattern was observed for major hurricanes except WK and SS major hurricanes had essentially the same average RMW while IN major hurricanes had the smallest average RMW. It is well understood that the RMW of a TC often contracts as it intensifies, as proposed in the convective ring model (Shapiro and Willoughby 1982), and expands as it is weakening. The extent to which the RMW contracts as it intensifies has recently been addressed by Stern et al. (2015) who showed that intensification continues after the contraction of the RMW ceases. The results presented in this study lack the temporal resolution to examine the evolution of the RMW. However, combining these statistics with the RMW sizes observed

Table 5.3: Composite kinematic statistics evaluated in each bin at the RMW using a centered 12 h intensity change. The composite-mean value at the RMW for each variable is given along with the standard deviation in parentheses. Statistically significant differences at the RMW can be observed in the Figures presented in chapter 3.

Bin	V $(m\ s^{-1})$	ζ $(10^{-4}\ s^{-1})$	I^2 $(10^{-6}\ s^{-2})$	M $(10^4\ m^2\ s^{-1})$	RMW (km)
Hurricanes					
WK	36.35 (6.92)	6.27 (5.49)	1.47 (2.91)	359.09 (214.33)	88.38 (49.90)
SS	36.69 (7.73)	7.03 (4.71)	1.55 (2.19)	305.29 (179.86)	74.09 (41.11)
IN	37.18 (5.84)	13.34 (9.27)	5.47 (10.06)	160.68 (121.62)	41.55 (31.21)
Major Hurricanes					
WK	51.22 (7.61)	21.40 (16.08)	14.52 (23.98)	190.47 (126.06)	37.39 (26.25)
SS	53.65 (6.34)	16.36 (7.18)	6.63 (7.35)	208.04 (83.05)	37.60 (13.35)
IN	53.82 (7.24)	21.87 (9.35)	11.58 (9.37)	159.76 (70.85)	29.47 (13.12)

in Figure 2.3 demonstrates that the average RMW of an IN hurricane or major hurricane is smallest when compared to SS and WK hurricanes or major hurricanes, respectively. This is in general agreement with results presented by Xu and Wang (2015) who showed that intensification rates were negatively correlated with RMW size. Although intensification rates were not examined in this study beyond the threshold criteria used to bin the data, the results suggest that TCs with a smaller RMW favor intensification at both hurricane and major hurricane intensity. It's interesting to note that this statement is particularly true at hurricane intensities where on average, IN hurricanes had an ∼30–50 km smaller RMW size compared to SS or WK hurricanes.

Table 5.4: Composite thermodynamic statistics evaluated in each bin at the RMW using a centered 12 h intensity change. The composite-mean value at the RMW is given for each variable along with the standard deviation in parentheses. Statistically significant differences at the RMW can be observed in the Figures presented in chapter 4.

Bin	T (K)	T_d (K)	T_{dd} (K)	θ_e (K)
Hurricanes				
WK	283.56 (1.47)	281.13 (2.47)	2.43 (1.89)	345.49 (6.28)
SS	284.08 (1.31)	282.38 (1.86)	1.70 (1.48)	348.79 (5.21)
IN	284.28 (1.39)	282.95 (1.55)	1.33 (1.20)	350.15 (4.80)
Major Hurricanes				
WK	285.94 (1.60)	284.02 (1.90)	1.92 (1.44)	355.10 (6.18)
SS	285.30 (1.55)	283.86 (1.94)	1.44 (1.75)	353.88 (5.62)
IN	285.02 (1.19)	284.11 (1.16)	0.91 (0.97)	353.95 (3.93)

CHAPTER 6
SUMMARY AND CONCLUSIONS

Flight level data obtained from the FLIGHT+ dataset (Vigh et al. 2016) were used to investigate the 700 hPa kinematic and thermodynamic structure of TCs stratified by intensity, intensity change, and age from 1999 to 2012. Composite-mean structures were created for hurricanes and major hurricanes that were weakening (WK), steady-state (SS), or intensifying (IN). The first hypothesis stated in section 1.2 was validated by demonstrating that both intensity and intensity change characteristics of TCs are important factors to consider when examining TC structure and therefore composite studies should consider both. Furthermore, the hypothesis that the age of the TC may additionally be related to structural differences was validated to a lesser extent.

The main findings reported in this study can be summarized as follows:

- IN TCs can be kinematically distinguished from WK or SS TCs by steep tangential wind gradients and a vorticity ring structure found radially inward of the RMW along with elevated inertial stability in that region, and weaker absolute angular momentum at all normalized radii.

- Overall, the thermodynamic structures demonstrated less differences compared to the kinematic structures. IN TCs were distinguished from SS or WK TCs by higher moisture content in the inner and outer-core regions. IN hurricanes possessed the highest θ_e at all radii compared to SS or WK hurricanes, although no significant pattern distinguishing major hurricanes was found for θ_e.

- WK major hurricanes also possessed the vorticity ring structure found in IN TCs. Furthermore, the vorticity ring structure was no longer present in late stage major hurricanes and was accompanied by a weakening of the tangential winds near the RMW. These collective results suggest these features were associated with physical processes involved in the breakdown of a PV ring described by Schubert et al. (1999) and observed by Kossin and Eastin (2001).

- Additional stratification of the results by TC age revealed that the tangential wind structural differences found in the eye of hurricanes manifested themselves more significantly at late stages in their life cycle whereas the tangential wind structural differences

in the outer-core of major hurricanes were primarily observed during early stages of their life cycle.

- Consideration of a previous and future 12 h intensity change demonstrated nearly the same kinematic structural differences found when using a centered 12 h intensity change. Thermodynamically, hurricanes exhibited more structural differences when observed with a future 12 h intensity change, providing further implications for TC intensity forecasting. On the other hand, major hurricane thermodynamic structural differences were more apparent based on the intensity change experienced in the previous 12 hours.

- Hurricanes exhibited more kinematic structural differences in the eye and near the RMW compared to major hurricanes which exhibited more kinematic structural differences in the outer-core region. These results suggest that there are distinct physical processes occurring in hurricanes and major hurricanes, and thus intensity must be considered when examining TC structure.

- Large scale parameters evaluated at the azimuthal mean time for each flight revealed differences for both hurricanes and major hurricanes (Table 5.2). These large scale differences were statistically significant in many cases for hurricanes, but essentially no significant differences were found for major hurricanes. Therefore, the large scale environment in which hurricanes are embedded may have a stronger impact on their structure when compared to major hurricanes, although further research would be required to verify this statement.

Results presented in this study confirm those found in previous literature that demonstrate structural differences between TCs when considering intensity (Mallen et al. 2005; Pendergrass and Willoughby 2009; Shapiro and Willoughby 1982; Vigh and Schubert 2009) and intensity change (Kossin and Eastin 2001; Rogers et al. 2013, 2015). The main composite-mean structural differences described in this section were statistically significant at the 5% level, suggesting that robust signals differentiating TCs stratified by intensity and intensity change can be observed which may benefit TC intensity forecasting. Additional work must be carried out to further identify the key physical processes that distinguish these groups of TCs. Although the composite approach taken in this study may have identified robust signals, we could only speculate on the main physical processes that were contributing to the observed structural differences.

Results from this study would therefore be greatly complemented by case studies examining the physical processes occurring in WK, SS, and IN hurricanes and major hurricanes. Furthermore, high resolution numerical simulations would greatly complement our findings, providing temporal resolutions that are often not available for observations. Future work will further test the robustness of the results presented after objectively removing TCs that possessed a concentric eyewall structure. Observations gathered throughout the full depth of the troposphere during the Tropical Cyclone Intensity (TCI) experiment funded by the Office of Naval Research will be examined to gain insight in regards to the main physical processes occurring as a TC intensifies, weakens, or remains steady-state. These observations may provide key information to further elucidate the results presented in this study.

BIBLIOGRAPHY

Barnes, G. M., J. F. Gamache, M. A. LeMone, and G. J. Stossmeister, 1981: A convective cell in a hurricane rainband. *Mon. Wea. Rev.*, **119**, 776–794.

Bolton, D., 1980: The computation of equivalent potential temperature. *Mon. Wea. Rev.*, **108**, 1046–1053, doi:10.1175/1520-0493(1980)108⟨1046:TCOEPT⟩2.0.CO;2.

Duchon, C. E., 1979: Lanczos filtering in one and two dimensions. *J. Appl. Meteor.*, **18**, 1016–1022, doi:10.1175/1520-0450(1979)018⟨1016:LFIOAT⟩2.0.CO;2.

Eastin, M. D., P. G. Black, and W. M. Gray, 2002: Flight level thermodynamic instrument wetting errors in hurricanes. Part I: Observations. *Mon. Wea. Rev.*, **130**, 825–841, doi:10.1175/1520-0493(2002)130⟨0825:FLTIWE⟩2.0.CO;2.

Gray, W. M. and D. J. Shea, 1973: The hurricane's inner core region. II. Thermal stability and dynamic characteristics. *J. Atmos. Sci.*, **30**, 1565–1576, doi:10.1175/1520-0469(1973)030⟨1565:THICRI⟩2.0.CO;2.

Kaplan, J. and M. DeMaria, 2003: Large-scale characteristics of rapidly intensifying tropical cyclones in the north atlantic basin. *Wea. Forecasting*, **18**, 1093–1108.

Kaplan, J., M. DeMaria, and J. A. Knaff, 2010: A revised tropical cyclone rapid intensification index for the north atlantic and eastern north pacific basins. *Wea. Forecasting*, **25**, 220–241, doi:10.1175/2009WAF2222280.1.

Kossin, J. P. and M. D. Eastin, 2001: Two distinct regimes in the kinematic and thermodynamic structure of the hurricane eye and eyewall. *J. Atmos. Sci.*, **58**, 1079–1090, doi:10.1175/1520-0469(2001)058⟨1079:TDRITK⟩2.0.CO;2.

Lee, W. C. and M. M. Bell, 2007: Rapid intensification, eyewall contraction, and breakdown of hurricane charley (2004) near landfall. *Geophys. Res. Lett.*, **34**, L02 802, doi:10.1029/2006GL027889.

Mallen, K. J., M. T. Montgomery, and B. Wang, 2005: Reexamining the near-core radial structure of the tropical cyclone primary circulation: Implications for vortex resiliency. *J. Atmos. Sci.*, **62**, 408–425, doi:10.1175/JAS-3377.1.

Pendergrass, A. G. and H. E. Willoughby, 2009: Diabatically induced secondary flows in tropical cyclones. Part I: Quasi-steady forcing. *Mon. Wea. Rev.*, **137**, 805–821, doi:10.1175/2008MWR2657.1.

Rogers, R., P. Reasor, and S. Lorsolo, 2013: Airborne doppler observations of the inner-core structural differences between intensifying and steady state tropical cyclones. *Mon. Wea. Rev.*, **141**, 2970–2991, doi:10.1175/MWR-D-12-00357.1.

Rogers, R. F., P. D. Reasor, and J. A. Zhang, 2015: Multiscale structure and evolution of hurricane earl (2010) during rapid intensification. *Mon. Wea. Rev.*, **143**, 536–562, doi:10.1175/MWR-D-14-00175.1.

Schubert, W. H. and J. J. Hack, 1982: Inertial stability and tropical cyclone development. *J. Atmos. Sci.*, **39**, 1687–1697.

Schubert, W. H., M. T. Montgomery, R. K. Taft, T. A. Guinn, S. R. Fulton, J. P. Kossin, and J. P. Edwards, 1999: Polygonal eyewalls, asymmetric eye contraction, and potential vorticity mixing in hurricanes. *J. Atmos. Sci.*, **56**, 1197–1223, doi:10.1175/1520-0469(1999)056⟨1197:PEAECA⟩2.0.CO;2.

Shapiro, L. J. and H. E. Willoughby, 1982: The response of balanced hurricanes to local sources of heat and momentum. *J. Atmos. Sci.*, **39**, 378–394.

Shea, D. J. and W. M. Gray, 1973: The hurricane's inner core region. I. Symmetric and asymmetric structure. *J. Atmos. Sci.*, **30**, 1544–1564, doi:10.1175/1520-0469(1973)030⟨1544:THICRI⟩2.0.CO;2.

Sitkowski, M., J. P. Kossin, and C. M. Rozoff, 2011: Intensity and structure changes during hurricane eyewall replacement cycles. *Mon. Wea. Rev.*, **139**, 3829–3847, doi:10.1175/MWR-D-11-00034.1.

Stern, D. P., J. L. Vigh, D. S. Nolan, and F. Zhang, 2015: Revisiting the relationship between eyewall contraction and intensification. *J. Atmos. Sci.*, **72**, 1283–1306, doi:10.1175/JAS-D-14-0261.1.

Vigh, J. L., N. M. Dorst, C. L. Williams, E. W. Uhlhorn, H. E. Willoughby, and F. D. Marks Jr., 2016: FLIGHT+: The extended flight level dataset for tropical cyclones (version 1.0). Tropical Cyclone Data Project, National Center for Atmospheric

Research, Research Applications Laboratory, Boulder, Colorado., [Available online at: http://dx.doi.org/10.5065/D6WS8R93.] Accessed 06 Jan 2016.

Vigh, J. L. and W. H. Schubert, 2009: Rapid development of the tropical cyclone warm core. *J. Atmos. Sci.*, **66**, 3335–3350, doi:10.1175/2009JAS3092.1.

Wilks, D. S., 2011: *Statistical methods in the atmospheric sciences*, International Geophysics Series, Vol. 100. 3d ed., Academic Press, 676 pp.

Willoughby, H. E., 1990: Temporal changes of the primary circulation in tropical cyclones. *J. Atmos. Sci.*, **47**, 242–264.

Willoughby, H. E. and M. B. Chelmow, 1982: Objective determination of hurricane tracks from aircraft observations. *Mon. Wea. Rev.*, **110**, 1298–1305.

Willoughby, H. E., J. A. Clos, and M. G. Shoreibah, 1982: Concentric eye walls, secondary wind maxima, and evolution of the hurricane vortex. *J. Atmos. Sci.*, **39**, 395–411.

Xu, J. and Y. Wang, 2015: A statistical analysis on the dependence of tropical cyclone intensification rate on the storm intensity and size in the north atlantic. *Wea. Forecasting*, **30**, 692–701, doi:http://dx.doi.org/10.1175/WAF-D-14-00141.1.

Zipser, E. J., R. J. Meitin, and M. A. LeMone, 1981: Mesoscale motion fields associated with slowly moving gate convective band. *J. Atmos. Sci.*, **38**, 1725–1750.